A GAP CALCULATION METHOD TO MINIMIZE INDUCTANCE DROP DURING REFLOW ON LOW COST HIGH CURRENT HELICAL WOUND PLANAR POWER INDUCTOR

Thirakaran Mahalingam

108867C

Degree of Master of Science

Department of Electrical Engineering

University of Moratuwa

Sri Lanka

May 2015

A GAP CALCULATION METHOD TO MINIMIZE INDUCTANCE DROP DURING REFLOW ON LOW COST HIGH CURRENT HELICAL WOUND PLANAR POWER INDUCTOR

Thirakaran Mahalingam

108867C

Dissertation submitted in partial fulfillment of the requirements for the degree Master of Science

Department of Electrical Engineering

University of Moratuwa

Sri Lanka

May 2015

DECLARATION

I declare that this is my own work and this dissertation does not incorporate without acknowledgement any material previously submitted for a degree or diploma in any other university or institute of higher learning and to the best of my knowledge and believe it does not contain any material previously published or written by another person except where the acknowledgement is made in the text.

Also, I hereby grant to University of Moratuwa the non-exclusive right to reproduce and distribute my thesis, in whole or in part in print electronic or other media. I retain the right to use this content in whole or part in future works (such as articles or books).

Signature: Date:

Thirakaran Mahalingam

The above candidate has carried out research for the Master Dissertation under my supervision.

Signature of Supervisor: Date:

Dr. D.P.Chandima

ABSTRACT

Power inductors are widely used in many power electronic applications such as voltage regulator modules, DC-DC converters and battery power systems. Recently electronic industry advancement shows an increasing trend in usage of low cost high current helical wound planar power inductors also known as processed power inductors. The new trend and competition in electronic industry is initiating to design and manufacture power inductors in high volume in a short processing time. The quasi-planar winding technique gives compact size and rectangular cross section is giving low heat dissipation while reducing AC/DC resistance. The above significance and requirement tend to design custom made different rating inductors. There is a problem in these types of inductors, a inductance drop after reflow soldering process as mostly these inductors are surface mount device. This is happening due to inadequate gap between helical wound coil conductor and upper core inner surface. The inadequate gaps are not only causing inductance drop, beyond that core separation as well. Therefore formulating an iterative equation to calculate gap to minimize and control inductance drop during reflow and operation for different rated power inductors during design and manufacturing stages will give a prominent solutions for processed inductor designers and manufacturers. The methodology is mathematically model the reflow and operational thermal model and calculate thermal directional strain that to be analyzed with ANSYS thermal simulation. Geometrically different five inductor models are selected. The inductance readings are recorded at both pre and post reflow simulation to calculate variation. The influencing parameters are identified with respect to core geometry, copper volume and dimension, direct exposing area of material to the thermal load during reflow and operations conditions considered as well. The samples have arranged with respect to inductance drop in an increasing manner and identified parameters have plotted along with inductance drop to find trends lines. The trend line relationships are combined together to formulate equation with a constant. The equations have validated with samples.

DEDICATION

To my wife and Etal Group (PVT) Ltd

ACKNOWLEDGEMENT

This endeavor would not have been a success unless I have the enormous support and guidance from my Research Supervisor Dr. D.P Chandima, Senior Lecturer, Department of Electrical Engineering, Faculty of Engineering, University of Moratuwa. The entire resources given for the research is ETAL Group (PVT) Ltd. I would like to take the opportunity to give my acknowledgement to Mr. Scott Lee Robinson, General Manager of the company for his support throughout the research. Last but not least, I would like to thank all the valuable supports that I had to make the event a success along with Electrical department of Faculty of Engineering, University of Moratuwa.

TABLE OF CONTENT

LIST OF FIGURES

LIST OF TABLES

LIST OF ABBREVIATIONS

AC	-Alternating Current
DC	-Direct Current
VHF	-Very High Frequency
FM	-Frequency Modulation
JEDEC	-Joint Electronic Device Engineering Council
SMD	-Surface Mount Devices
FEM	-Finite Element Method
IR	-Infrared
SMT	-Surface Mount Technology
CAD	-Computer Aided Design
PCB	-Printed Circuit Board
3D	-Three dimensional
SST	-Steady State Thermal
L drop	-Inductance drop
NPI	-New Product Introduction

Chapter 01

1.0 INTRODUCTION:

Inductor is an electronic component which is widely used in many power electronic applications. An inductor is a passive device consisting of one or more turns of the wire used for its inductance function or opposes change in current [1]. Inductors are components that are simple in their construction consisting of coils of insulated copper wire wound around a former. That will have some type of core in its center. The core might be a metal such as iron that can be easily magnetized or in high frequency inductors it will likely to be air [1]. Another name used for an inductor is a "Choke". Inductors, being just coils of copper wire, will allow DC to pass easily, but when AC is applied, inductors create an opposition to current flow that increases, as the frequency of the alternating current increases. Therefore AC is prevented from flowing or is "Choked off" while DC is allowed to pass. This effect is used in power supply circuits where the public AC mains (line) supply has to be converted to a DC supply suitable for powering electronic circuits [1]. There are plenty of conventional inductors those are used in electronic circuits. Some inductor models used in particular applications have discussed as following.

An air cored inductors as shown in figure 1.1 are used in many circuits operating in the 1MHz to several hundred MHz range, including VHF FM radios and TV receivers.

Figure 1.1: An air cored inductor

Figure 1.2: A toroidal inductor

Source: www.learnabout-electronics.org

The Surface mounted multi-layer chip inductors are tiny; often only 3 or 4mm across. Although this physical size limits the values of inductance that can be achieved, typical values of less than 1nH up to a few hundred nH are useful for many radio frequency and communications applications. The example shown is part of a hard disk drive control circuit as shown in figure 1.3.

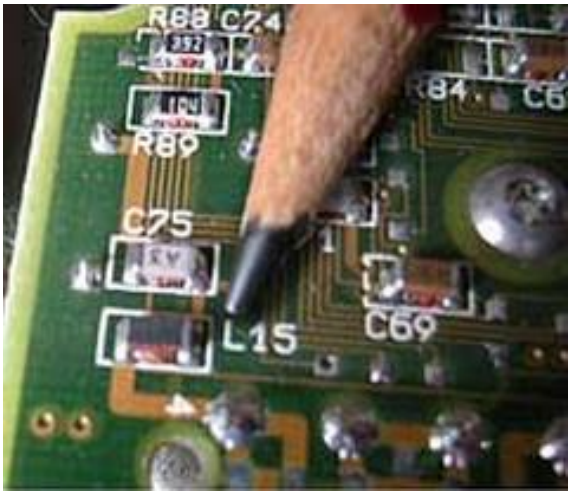

Figure 1.3: Multilayer chip inductor

Source: www.learnabout-electronics.org

Figure 1.4: Helical wound planar inductors

Source: www.coilws.com

Recently the electronic industry advancement shows an increasing trend in usage of low cost, high current helical wound planar power inductors also known as processed

power inductors as shown in figure 1.4 in their various applications, because of its high current handling performance at high frequencies as well as the low material and manufacturing costs[4]. The rectangular cross section conductors are used rather than round conductors and this is adversely reducing the AC/DC resistance, eventually causing lower heat dissipation during operation[5]-[13]. The new Quasi planar winding construction technique gives the compact size. These inductors are widely used in voltage regular modules, DC-DC converters and battery power systems. The above significance and the requirements tend to design custom made, different rating inductors. There is a problem in these types of inductors on inductance drop after reflow oven soldering process as mostly these all inductors are Surface Mount Devices. This is happening due to inadequate gap between the helical wound coil conductor and upper core's inner surface. The inadequate gaps are not only causing inductance drop, beyond that they are causing core separation as well as shown in figure 1.5.

Core separation after reflow simulation

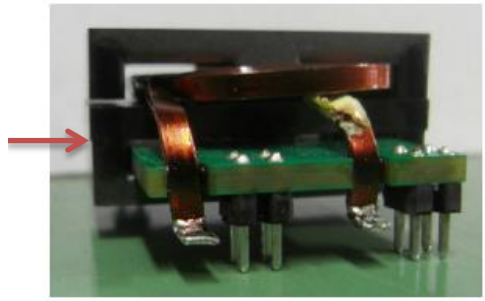

Figure 1.5: The core separation found due to inadequate gap between copper coil and core in a module

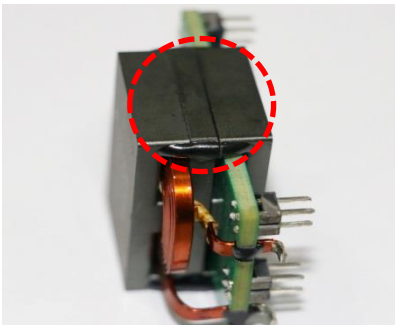

Figure 1.6: A minor separation found due to inadequate gap between copper coil and core in a module

In an inductor the core flux is decided only by the load current. Thus if the load current increases, there is a possibility that the core may saturate and inductance will come down. So the primary consideration in an inductor is that one has to know the maximum load current and have the core which does not saturate at this current. This can lead to a large core size if the current to be handled is large. The core size can be reduced considerably by introducing an appropriate air gap in the magnetic circuit. This gives high load current carrying capacity before the magnetic material get saturation and knows as DC bias characteristics of inductor [22].

The exemplary description of B-H curve of a magnetic core with and without air gap is shown is figure 1.7

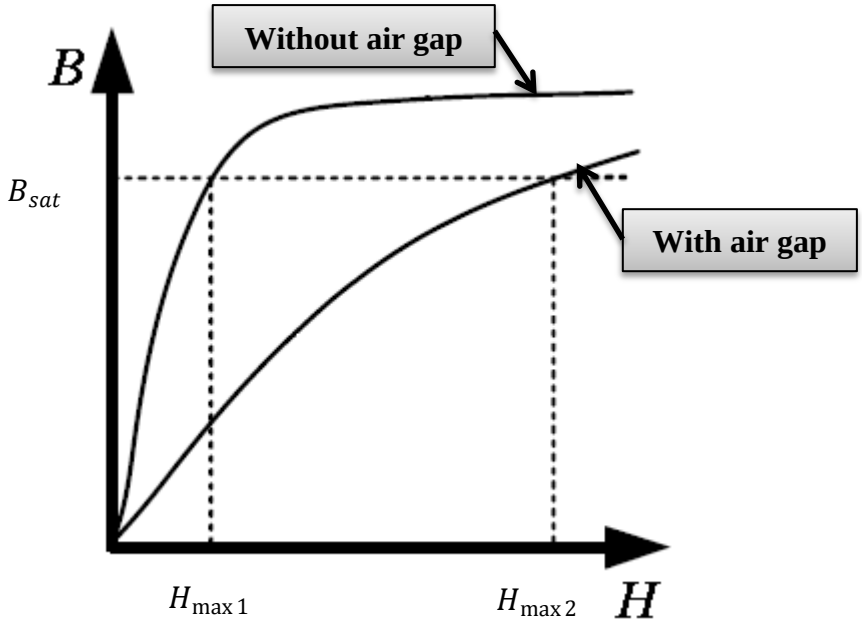

Figure 1.7: Comparison of B-H curve for magnetic core without and with air gap

Let us consider an EI inductor and the influence of air gap on inductance value, which is giving the exact reason for the study to maintain the gap to minimize or control the inductance drop due the thermal load.

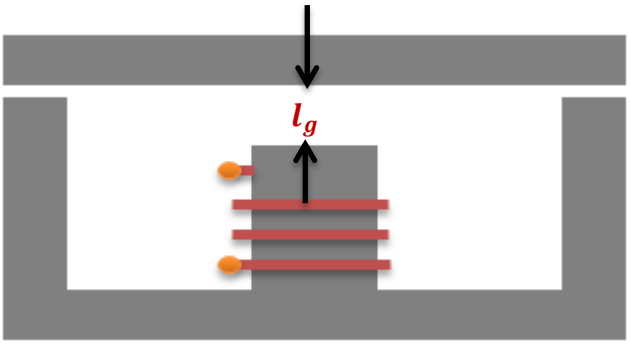

Figure 1.8: Inductor geometry with E I core

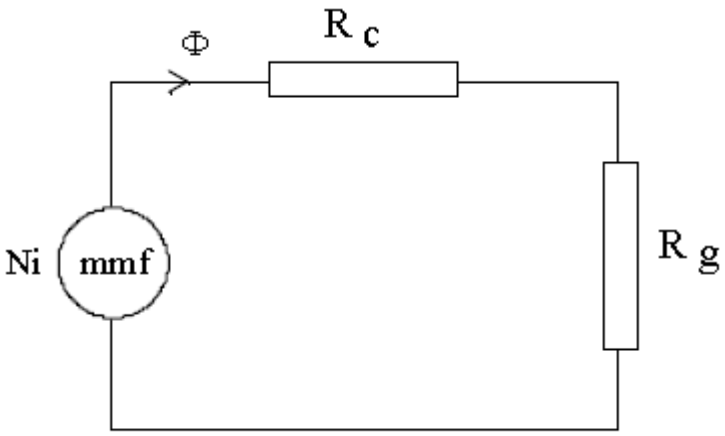

Figure 1.9: Model of magnetic circuit for the inductor

Using faradays law,

$$e = N \cdot \frac{d\emptyset}{dt} \tag{1}$$

Where e is the induced electromagnetic force, N is number of turns in winding and $\frac{d\emptyset}{dt}$ is rate of change of flux density.

From the equivalent magnetic circuit in figure 1.9, the R_c is core reluctance and R_g is air gap reluctance.

It is given the core reluctance and air gap reluctance as following in equations (2) and (3)

$$R_c = \frac{l_c}{\mu_0.\mu_r.A_c} \tag{2}$$

$$R_g = \frac{l_g}{\mu_0.A_c} \tag{3}$$

where,

μ_0 - permeability of air (H/m)

μ_r - relative permeability of core material

l_c - mean magnetic path length in magnetic material / m

l_g - air gap length / m

A_c - core cross sectional area / m^2

Assuming the area of cross sections of the core and air gap to be equal, that is neglecting fringing flux in the model magnetic circuit of the inductor.

$$\emptyset = \frac{mmf}{R_c+R_g} \tag{4}$$

$$\emptyset = \frac{Ni}{\frac{l_c}{\mu_0.\mu_r.A_c}+\frac{l_g}{\mu_0.A_c}} \tag{5}$$

$$e = \left[\frac{N^2}{\frac{l_c}{\mu_0.\mu_r.A_c}+\frac{l_g}{\mu_0.A_c}}\right].\frac{di}{dt} \tag{6}$$

$$e = L\,.\frac{di}{dt} \tag{7}$$

$$L = \frac{N^2}{\frac{l_c}{\mu_0.\mu_r.A_c}+\frac{l_g}{\mu_0.A_c}} \tag{8}$$

where,

L - inductance value of inductor / H

$\emptyset$ - magnetic flux / weber

i - rms current in winding / A

For simplicity it is considered as high permeability core,

$$\frac{l_g}{\mu_0 . A_c} \gg \frac{l_c}{\mu_0 . \mu_r . A_c}$$

$$L = \frac{\mu_0 . A_c N^2}{l_g} \tag{9}$$

The equation 09 is shown apparently that inductance is inverse proportionate for air gap. Therefore maintaining the air gap length will eventually lead to minimize or control the inductance drop due to thermal load.

These gaps are already calculated during design stage and prepared specification to manufacture the same. But there should some other factors influencing thermal expansion due to thermal stress applied on components. The inductance drop can happen only if pre ground gap on center leg of ferrite core increased. Normally the epoxy used for assembling purpose of miniature transformers and inductors are well capable of maintaining gap during reflow soldering and it has been using since last two decades. But the gap should compensate conductor coil and core expansion. There is not available a simplified way to calculate approximate gap to minimize or control the inductance drop in analytical method. Designers are using trial and error method or individually doing FEM analysis to overcome the problem. This takes a longer time frame to conclude a complete design and with the increasing trend on demand, designers cannot take longer time to give a solution to customers. In some circumstances, if the gap is high, problem can be solved, but different rating with similar geometry will not be possible with calculation, which leads the designer to try with another different geometry type in order to design the inductor to fulfill customer requirement.

The target is to formulate an iterative equation to calculate gap to minimize and control inductance drop during reflow and operation for different rated power

inductors during design and manufacturing stages. There are two scenarios analyzed, where planar power inductors can be subjected to thermal loads. First is during the reflow soldering and second the operational condition as a DC/AC current inductor. In the second situation, for AC condition the simplified model is used with approximate percentage of ripple current from DC current to calculate the heat dissipation. The thermodynamics concepts have used to analyze both scenarios. Firstly, the reflow model is studied and analytical mathematical model is developed to find out temperature profile on a specified planar power inductor. The all three heat transfer mechanisms are involved in a reflow model, where the convection and radiation have involved in reflow oven and conduction is in component. Equating the thermal energy transferring rate analytical mathematical model is developed and temperature profile on component is calculated while considering Joint Electronic Device Engineering Council (JEDEC) soldering profile in Surface mount Device (SMD) type components [15]. This profile have verified with model inductor in reflow oven with DATAPAQ profile reader to ensure the mathematical model.

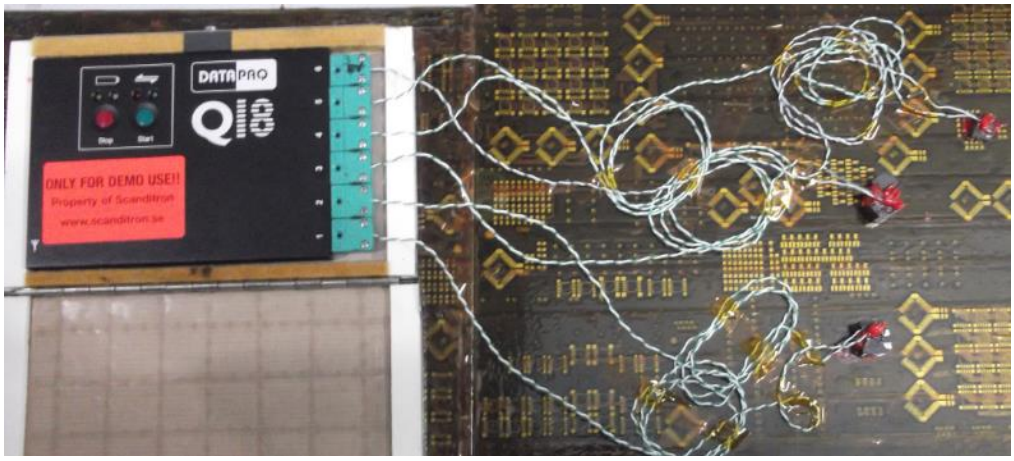

Figure 1.10: The DATAPAQ profile reader is connected with component surface with thermocouple

A CAD Finite Element Analysis performed for a model inductor that has developed in ANSYS 13.0 software. This has done to verify the direction of thermal strain that causing the push when subjected to thermal load in both reflow and operational conditions [14]. The internal heat generation due to core and copper loss has been

considered for evaluating the operational condition. The results of FEM analysis have compared and concluded the highest thermal strain can happen during reflow soldering process and along vertical axis (Z axis).

Five types of inductors as RM8, PQ16, ER25 and ER12.7 two different models are selected with fifty products in each are used to analyze the behavior on several influencing variable parameters. A set of variable parameters has been identified with respect to geometry and construction of those planar helical wound planar inductors. The parameters are noted down before and after reflow condition. The major influencing parameters are identified and rests have been omitted for further analysis. The behavior of identified parameters has been plotted against inductance drop in increasing manner and observed trend. Then relationships have been created against inductance drop. The found relationships have been merged together with a constant to formulate iterative equation. By using the five proto type samples with different geometry constant value is calculated for each model.

The formulated equation has been validated with an ER12.7 inductor model and the validation of results was presented in the thesis.

Chapter 2

2.0 REFLOW OVEN THERMAL MODEL AND TEMPERATURE DISTRIBUTION

Reflow oven soldering process is a process used in Surface Mount Technology (SMT) to soldered Surface Mount Components in Printed Circuit Boards (PCB) under a control transient thermal profile.

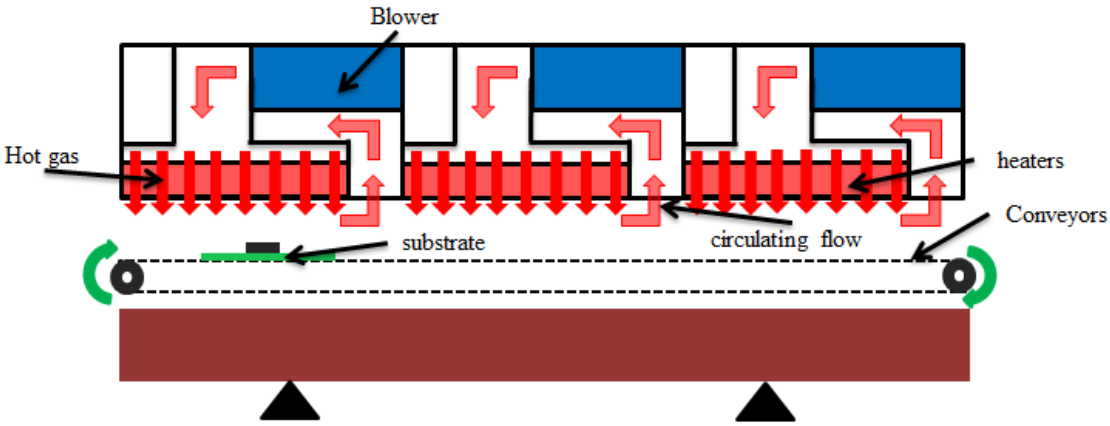

Figure 2.1: Simplified model of a reflow soldering oven

2.1 Modes of heat transfer in reflow soldering oven:

There are three different heat transfer modes involved in most SMT reflow ovens [16]-[17]. They are conduction, convection and infrared radiation (IR). In most of the reflow ovens the predominant heat transfer method is convection. But other modes are contributing in transferring heat to the product. The heat transferring process happens only when there is a temperature difference between products. In general the greater the temperature difference, the higher the heat transfer rate.

2.1.1 Conduction heat transfer:

Conduction heat transfer occurs when two solid masses of different temperatures are in contact with each other [18]. Conduction also occurs within the same mass if a

temperature differential exists within the mass. The rate of heat transfer depends on thermal conductivity of the materials and geometric factors such as thickness and contact area.

The temperature gradient within a homogeneous substance results in an energy transfer rate within the medium which can be calculated by Fourier's Law

$$q = -kA\frac{\partial T}{\partial x} \tag{10}$$

where,

$q = \text{Heat tranfer rate } (W)$

$k = \text{Thermal conductivity } \left(\frac{W}{mK}\right)$

$A = \text{Area } (m^2)$

$\frac{\partial T}{\partial x} = \text{Temperature gradient in direction normal to area } A$

Conduction can both help and hinder the SMT reflow process. This helps uniform product heating, as heat will conduct from a hot spot to a cold spot in the product.

2.1.2 Convection heat transfer:

Most reflow ovens today used forced convection as the primary heat transfer mode. Convection heat transfer occurs when a fluid (such as air, nitrogen, or water) passes over an object (such as an SMT assembly). Convection heating or cooling requires contact of the flow with the solid part. Only the layer of the flow that is in contact with the part is actually transferring heat. Convection may be classified as natural or forced.

Natural convection occurs when no flow is being forced over the object [18]. Forced convection requires an external force that pushes or pulls the flow over the object. Typically, forced convection heating or cooling rates are higher than natural convection rates.

If the upstream temperature of the fluid is T_∞ and the surface temperature of solid is T_s the heat transfer per unit time is given by Newton's Law of cooling;

$$q = hA(T_s - T_\infty) \tag{11}$$

where,

$q =$ heat transfer rate by convection (W)

$h =$ convection heat transfer co $-$ efficient $\left(\frac{W}{m^2K}\right)$

$A =$ surface Area (m^2)

2.1.3 Infrared Radiation:

The third mode of heat transmission is due to electromagnetic wave propagation, which can occur in a total vacuum as well as in a medium [18]. Experimental evidence indicates that radial heat transfer is proportional to the fourth power of the absolute temperature, whereas conduction and convection are proportional to a linear temperature difference.

The fundamental Stefan Boltzmann Law:

$$q = \sigma\varepsilon T^4 \tag{12}$$

where,

$\varepsilon =$ Emissivity of the surface

$\sigma =$ Boltzmann contant, independent of surface medium and temperature

Infrared Radiation (IR) occurs when two bodies of different temperature are insight of each other.

$$q = \sigma\varepsilon A(T_s^4 - T_{sur}^4) \tag{13}$$

where,

$T_s^4 =$ Surface temperature (K)

$T_{sur}^4 =$ Surrounding temperature (K)

2.2 Analytical model:

The thermal analysis of high current helical wound planar inductor is considered as one component in a PCB for analytical purpose as shown in figure.

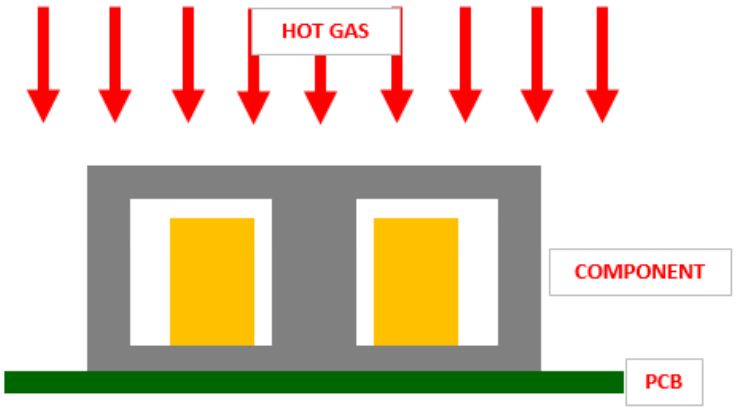

Figure 2.2: The way of product subjected to thermal load during reflow processes

Heat along top to bottom side is considered. As first approach one-dimensional analytical model was developed. Because of large uniform heat transfer by convection along the depth of the structure (Z-direction), heat transfer is assumed only to take place in this direction on product.

Conduction in X and Y direction is neglected and a temperature gradient along the Z direction is not taken into account either.

The assumptions made to develop the analytical model for substrate heating are as follows,

- The primary factors affecting the heat transfer co efficient are the gas flow parameters, Flow rate, density and pressure of the heater gas
- The exact measurement of these parameters is too complicate, because of the extreme circumstance in the reflow oven (such as small space, high temperature)
- The alternative solution is the examination of heating capability of the oven

- In this analysis a model heat transfer co-efficient in a forced convection reflow oven is considered
- Considering the construction of "forced convection reflow ovens", the radiation heat load is neglected
- Under the forced air convection heating the components & PCB will not be heated beyond the temperature of hot gas

The absorbed thermal energy during soldering is as following [3];

$$Q_a = Q_c + Q_k \tag{14}$$

where,

$Q_a =$ Absorbed thermal energy
$Q_c =$ Convection heat
$Q_k =$ Conduction heat

By equating the heat transfer flow rate the below equation can be obtained;

$$Q = h.A\left(T_g - T_c\right) = \rho.V.C_p \frac{\partial T_c}{\partial t} \tag{15}$$

where,

- Surface Area – A m^2
- Volume of the substrate /Component – Vm^3
- Hot gas temperature - T_g ℃
- Assume, Substrate/component Temp - T_c ℃
- Heat flow rate - $Q\ W/m^2$
- Heat transfer co-efficient - $h\ W/m^2K$
- Density of substrate/component - C_p J/kg/k

This is a 1st order differential equation, by solving the above ODE

$$T_c = T_0 + (T_g - T_0)(1 - e^{-\frac{t}{\tau}}) \tag{16}$$

where,
$T_0 =$ intial temperature (℃)
$\tau \rightarrow$ time cosntant and given by

$$\tau = \frac{C_p \rho V}{hA}$$

All five samples were evaluated against the analytical thermal reflow profile and real simulation with DATAPAQ as shown in below picture. The obtain data is plotted against the analytical model to validate the analytical reflow mathematical model.

The convection heat transfer co-efficient are considered from below graph.

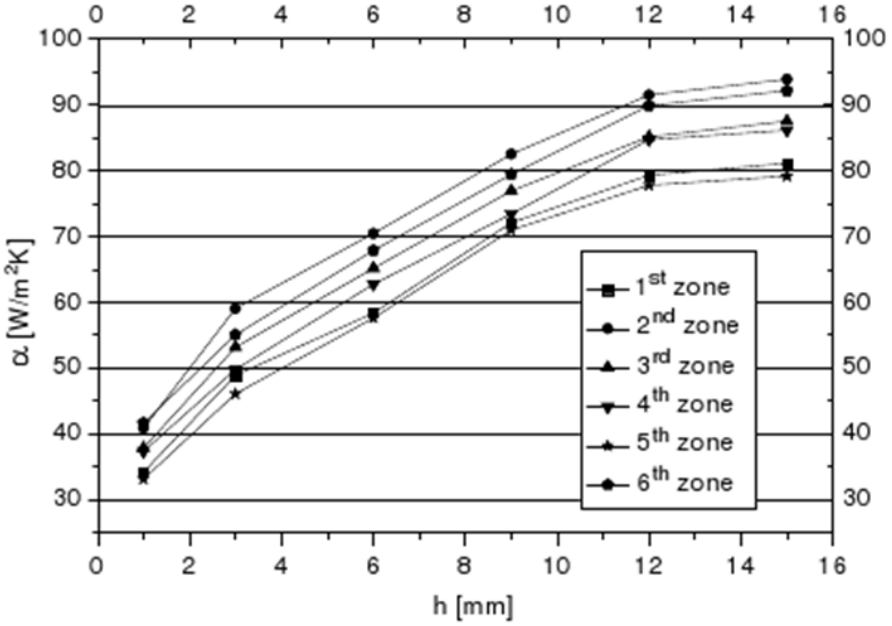

Figure 2.3: Convection heat transfer co efficient plot [19]

Table2.1: The required data to substitute on equation for all selected samples

Description		ER25 Ind.	PQ16 Ind.	ER12.7(1) Ind.	RM8 Ind.	ER12.1(2) Ind.
Ferrite	Volume (mm^3)	3195	1211	379	2158	370
	Exposed area (mm^2)	1040	605	250	457	228
Copper	Volume (mm^3)	791	408	132	658	88
	Exposed area (mm^2)	125	307	20	442	18
Height of product (mm)		10.48	11.99	5.86	13.65	5.03
Average heat transfer co-efficient (W/m^2 K)		81.5	85	63.5	87	60.5

Density of ferrite: 4800 kg/m^3

Density of copper: 8940 Kg/m^3

Specific Heat Capacity of ferrite: 750 J/KgK

Specific Heat Capacity of copper: 385 J/KgK

The temperature profiles on both calculated and real measured profile with DATAPAQ profile readers have described the variations.

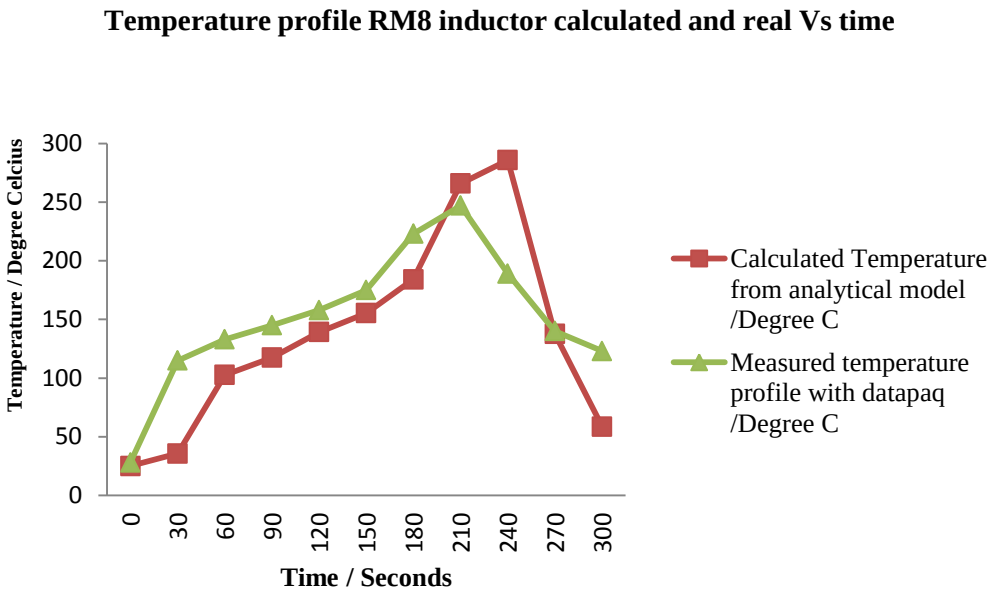

Figure 2.4: Plot of temperature profile of RM8 inductor calculated and real vs time

The calculated profile is higher than the measured profile for RM8 inductor. This can happen due to the reflow oven efficiency. The difference between calculated and measured values has approximately 30 degrees difference at peak conditions. The difference is showing that we have to have a profile evaluation on a specified reflow oven or this has to be evaluated at once in customers reflow oven in order to resolve the inductance drop analysis mismatches.

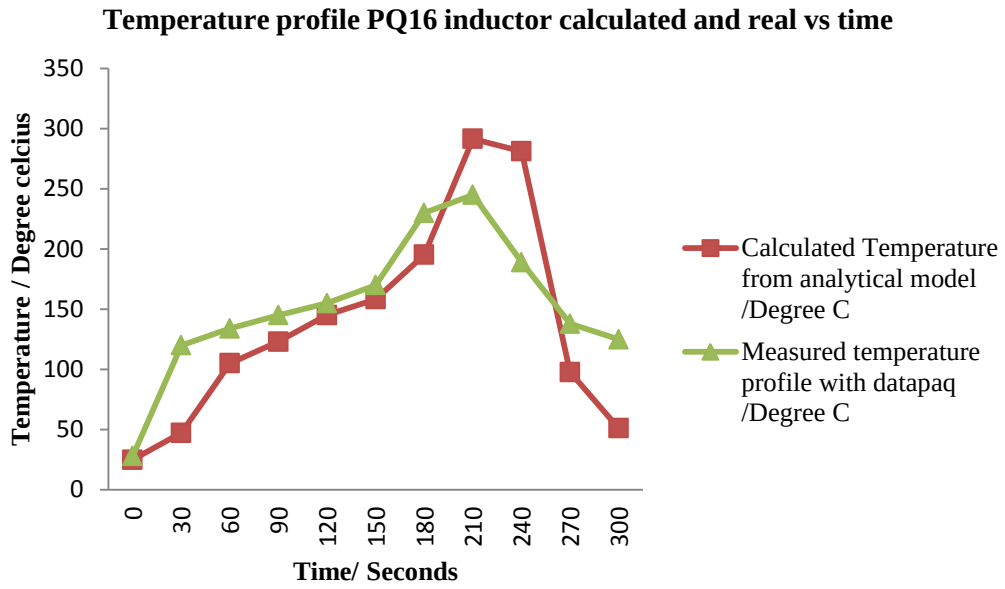

Figure 2.5: Plot of temperature profile of PQ16 inductor calculated and real vs time

The plot for PQ16 inductor is showing the same result as on RM8 inductor. The calculated temperature profile is higher than measured profile.

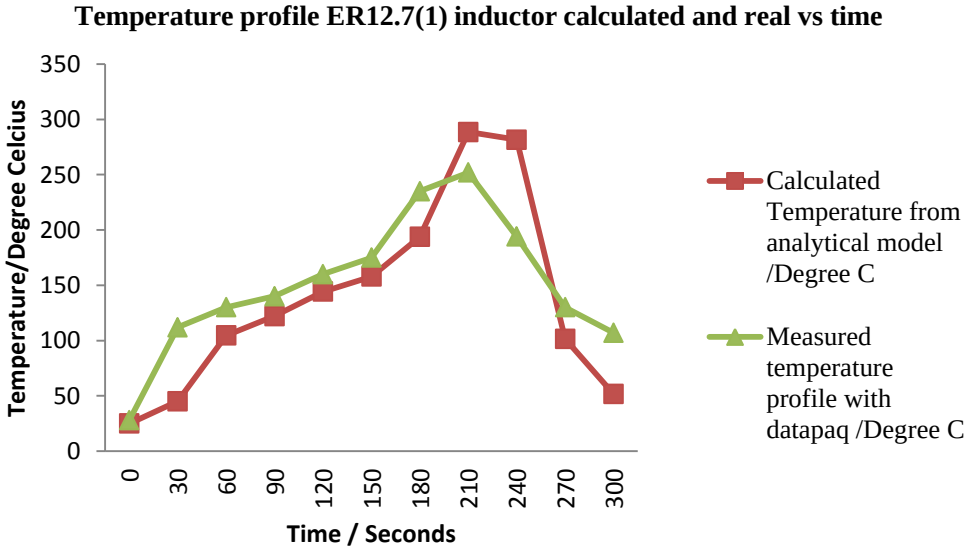

Figure 2.6: Plot of temperature profile of ER12.7 (1) inductor calculated and real vs time

The plot for ER12.7(1) inductor is showing the same result as other two inductor samples that the calculated value is higher than the measured value due to efficient drop of reflow oven. This can be happen due to life time of reflow oven used. When it gets old the capability of heaters and blowers may reduce.

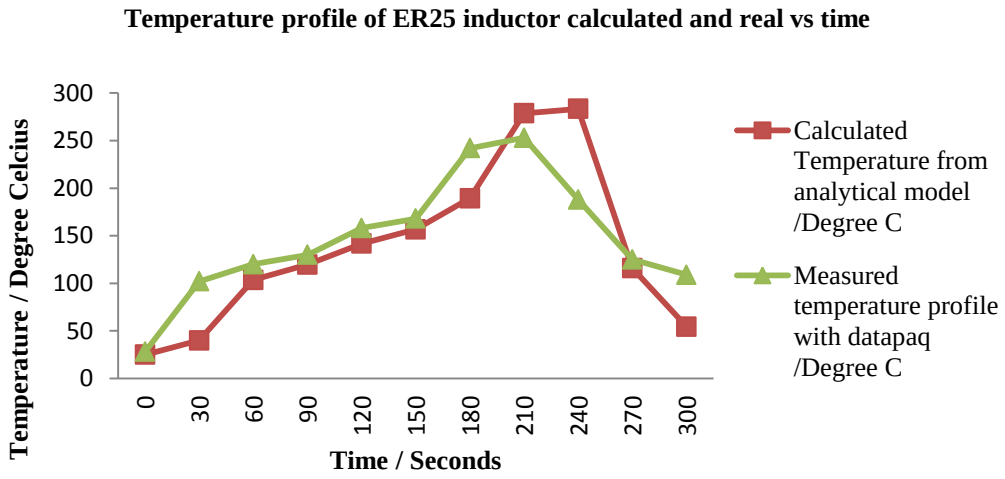

Figure 2.7: Plot of temperature profile of ER25 inductor calculated and real vs time

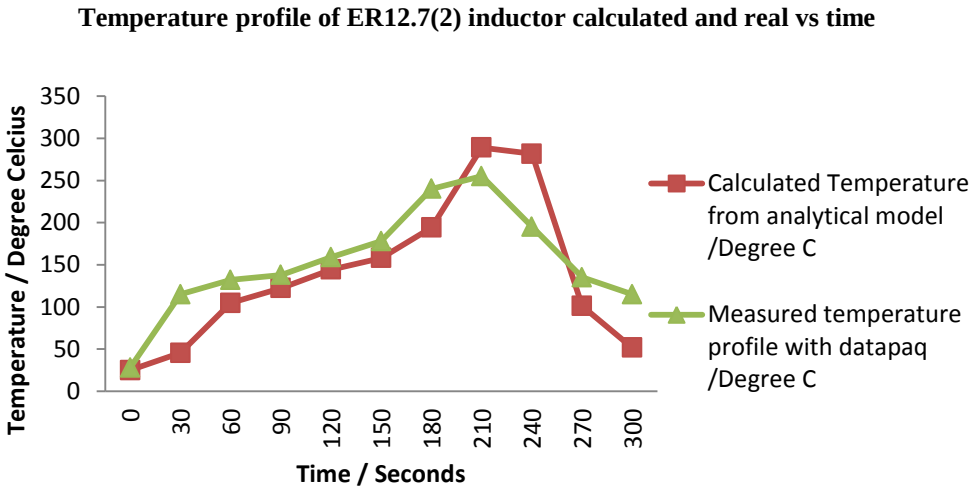

Figure 2.8: Plot of temperature profile of ER12.7 (2) inductor calculated and real vs time

The all inductors have shown the same result and it emphasis always the thermal load applied on product is lesser than calculated thermal load.

Chapter 3

3.0 THERMAL ANALYSIS OF AN INDUCTOR IN REFLOW AND AC/DC OPERATION CONDITION WITH ANSYS

A CAD model thermal analysis is conducted in order to identify the effect and influence of the thermal strain in all three axis (X, Y and Y). The main objective of this exercise is to identify the main axis influence. The analytical model of temperature gradient on component during the product subjected to thermal stress in reflow oven is proven in previous chapter. This FEM analysis is to verify that material is subjected to the highest thermal strain and in which axis. Simulation result can emphasize the reason of inductance drop. With the past history and the inductor design and manufacturing phenomenon is showing that the gap should be increased in order to give an inductance drop. This is possible only with the materials assembled, such as ferrite core, copper coil and epoxy should be subjected to a thermal load and the thermal stress should develop a thermal strain and also with respect to the geometry and the construction of the product, the axis also should influence a major role.

There are only three occasions where the product can be subjected to thermal load. Those are as following;

1. During the reflow oven soldering process
2. Induced thermal strain due to internal heat generation with DC/AC current in operation condition along with core loss.

3.1 Methodology:

The ANSYS 13.0 is used as CAD tool to solve the problem stated above. The following project schematic diagram is created in ANSYS [22].

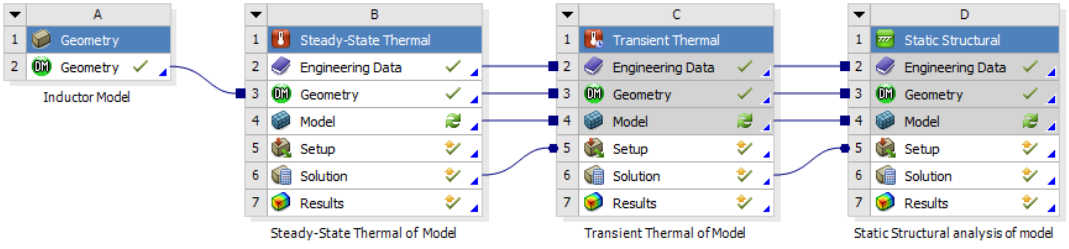

Figure 3.1: The project schematic diagram in ansys

The four analysis systems such as geometry, steady state thermal, transient thermal and static structural in ANSYS tool box are used to develop the project schematic. The purpose to select the four analysis systems are as following, see appendix J.

3.1.1 Geometry:

The geometry mode is to develop the inductor model that I am going to do the FEM analysis for thermal strain. The inductor model developed is shown in figure.

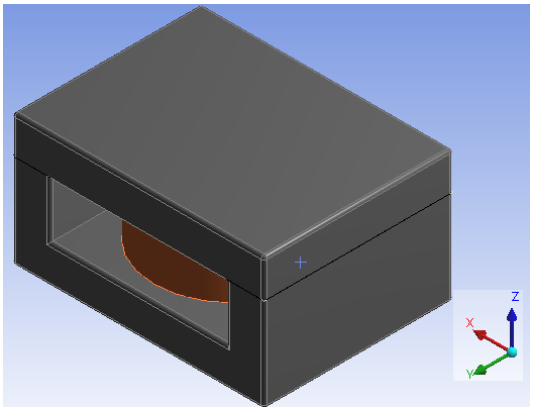

Figure 3.2: The developed Inductor CAD model for ANSYS thermal simulation

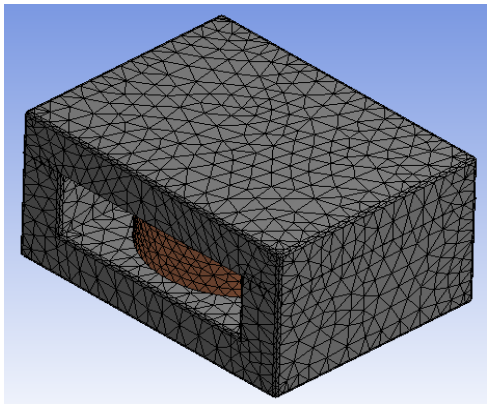

Figure 3.3: The meshed inductor model in order to conduct FEM for thermal analysis

The above geometry of an inductor is developed with an ER type E and I core and the helical wound coil with flat conductor and the E and I part is assembled with an epoxy which is used normally for transformer and inductor assembly.

The global coordinate system is used and the contact surface connections are considered as bonded. The assembled component is created with mesh in order to conduct the Finite Element Analysis. The meshed model is shown in the figure 3.3.

3.1.2 Steady State Thermal:

The steady state thermal analysis system is used to find out the temperature rise of the developed inductor in Steady State Thermal (SST) condition.

The convection heat transfer medium is considered and the average parallel and perpendicular flows are considered as 1560W/m^2 and 2175 W/m^2, as per the following resource [17]:

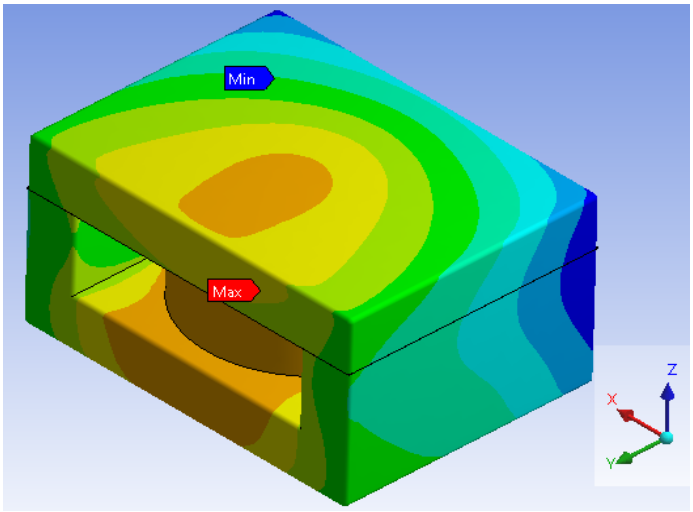

Figure 3.4: Steady state thermal analysis in ANSYS work bench for developed model

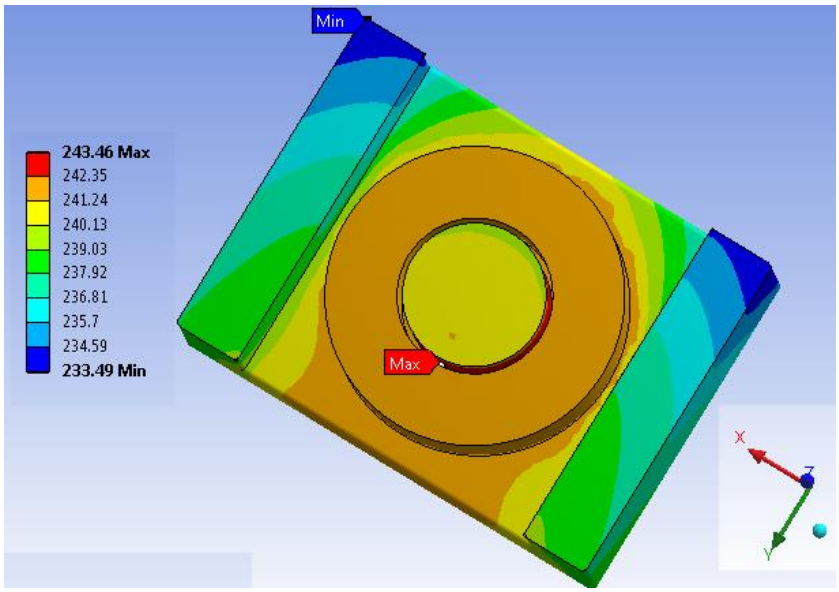

Figure 3.5: Steady state thermal simulation and maximum and minimum points

The steady state thermal analysis and the temperature rise is shown in the FEM model in figure 3.5. The maximum temperature rise (243 ^{0}C) happens in E ferrite core and minimum (233 ^{0}C) also in E core. This is due to the direction of model sent through the reflow and the effect of both parallel and perpendicular flows.

3.1.3 Transient Thermal:

The transient thermal analysis considered over 300 seconds, the temperature settings mentioned in table 3.1 is with respect to zones in reflow oven. There are 10 zone considered in the simulation as same as the reflow oven used to validation of the developed equation.

Table 3.1: The convection heat transfer co-efficient and zone temperature along with time

Time (Seconds)	0	30	60	90	120	150	180	210	240	270	300
Convection heat transfer co-efficient (W/m^{2}K) of 20 mm height product	78	79	80	81	82	81	81	82	82	50	50
Temperature (^{o}C)	25	100	110	130	150	160	200	300	280	90	50

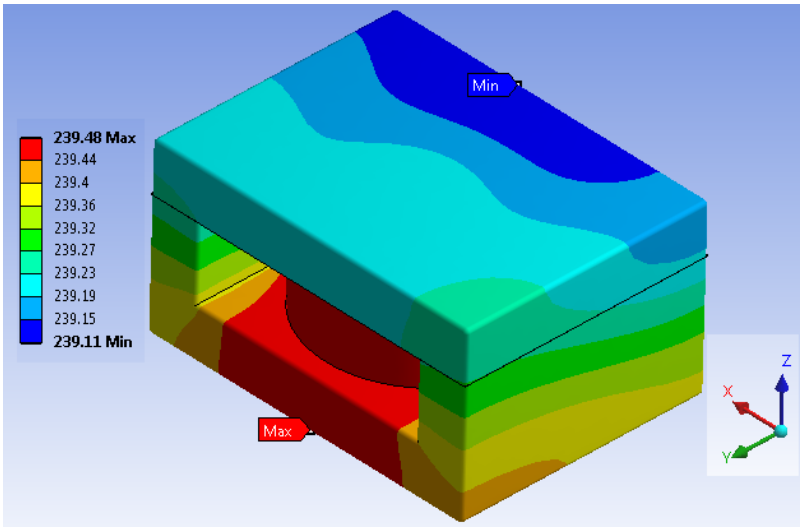

Figure 3.6: The transient thermal simulation and maximum and minimum points

The minimum and maximum temperature occurs in I and E ferrite cores. The convection heat transfer co-efficient is used as per table 3.1.

3.1.4 Static Structural:

The thermal strain on complete product has been checked for all three directions. The observed results are as following. The maximum thermal strain occurs at epoxy and minimum occurs in I core. The max is 0.01631 m/m and the minimum is 0.0021711 m/m.

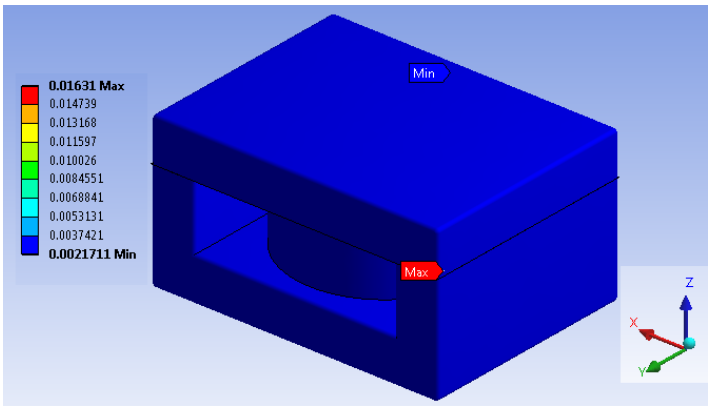

Figure 3.7: The static structural thermal strains and maximum and minimum points in Z direction

Table 3.2: The maximum and minimum thermal strain occurs with respect to direction, Y and Z direction

Direction	Max		Min	
	Occurs @	Value m/m	Occurs @	Value m/m
X	Epoxy	0.01631	I core	0.002171
Y	Epoxy	0.01631	I core	0.002171
Z	Epoxy	0.01631	I core	0.002171

The maximum and minimum thermal strain occurs as shown in figure 3.8. The maximum points or area is shown in red in color.

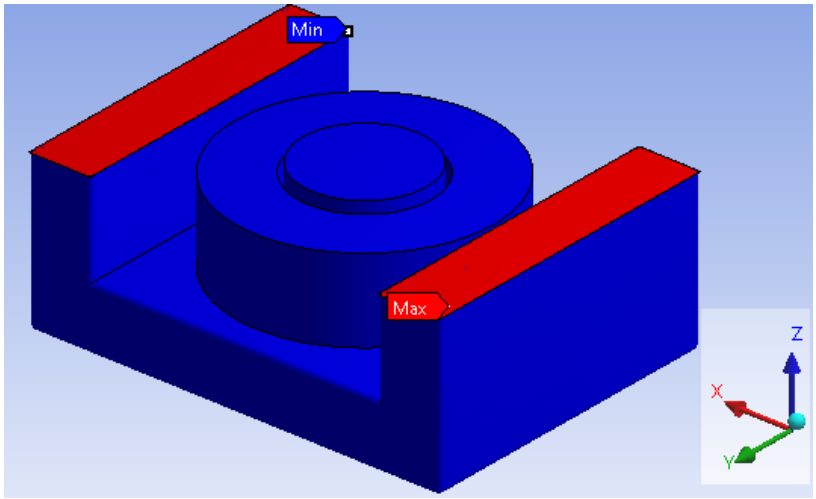

Figure 3.8: The static structural thermal strains and maximum and minimum points in Z direction

The directional deformation of complete product is shown in figure 23.

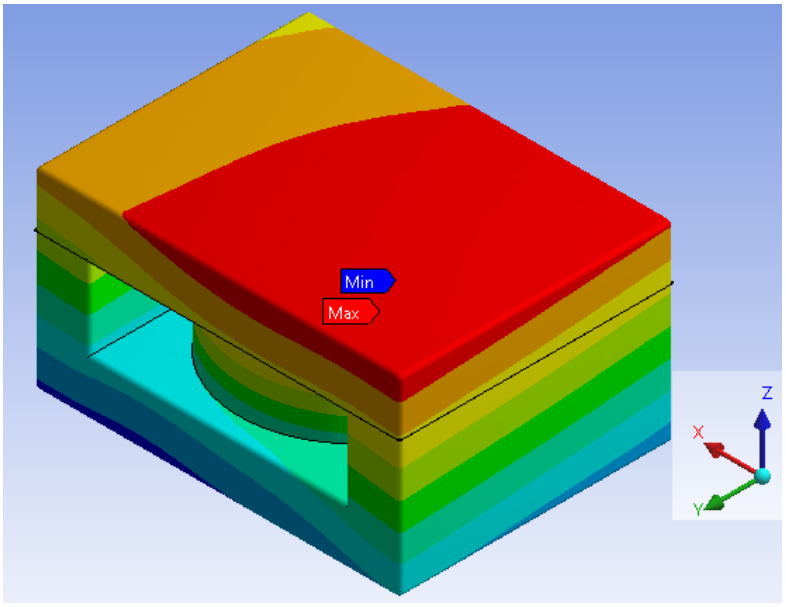

Figure 3.9: The directional deformation in Z direction due to transient thermal load applied on product

The maximum point is shown in figure 3.9 and it is in copper coil. This shows the tendency of pushup unless adequate gap is allowed.

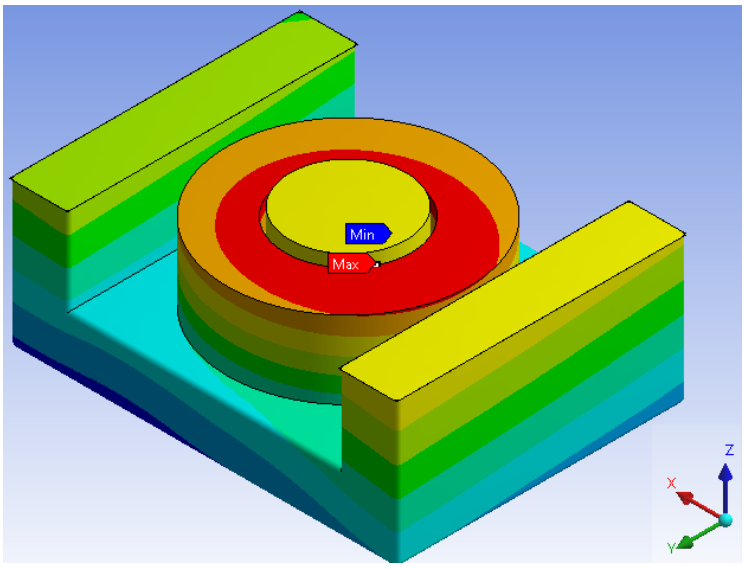

Figure 3.10: The directional deformation maximum point copper coil in Z direction due to transient thermal load applied on product

3.2 DC/AC operational condition of a helical wound planar power inductor

The same size of model inductor develop for reflow analysis has been used to simulate the operation condition [22]. The induced thermal strain due to internal heat generation of copper and core loss has been considered with both DC and AC situations to represent both DC/AC inductors.

The following parameters have considered for developing the prototype.

- The rated current applied on DC Bias condition is 20A
- The winding copper resistance is 2 Ohm
- The 40% increase of applied current is considered to check under AC current

The same analysis system was followed to do the thermal simulation as Geometry – Steady State Thermal Model – Transient Thermal – Static Structural to analyze the strain developed .As these models are considered in operational stage and more time was given in order to replicate the operation condition.

Under DC operation the maximum and minimum thermal strain happened is at epoxy glue between E core and copper coil and I core. Under AC operation the maximum and minimum thermal strain occurs at same point with different values.

The comparison in all three occasions have concluded as following table 3.3 and it has been shown for maximum thermal strain can subject on product during reflow soldering process. The inductor gap increase due to thermal expansion of copper conductor push up can occur during reflow soldering than operational condition

Table 3.3: The thermal strain comparison of all three occasional models during the inductor subjected to thermal load.

Models	Reflow model	DC inductor	AC inductor
Max. thermal strain in Z direction / (m/m)	0.014	0.00031	0.00038

Chapter 4

4.0 ITERATIVE EQUATION FORMATION AND VALIDATION:

There are five types of inductors selected for data collection. The inductance was measured using LCR meter. The five types of inductors are selected with different geometry. The five sample inductor types are as following,

- RM8 core inductor
- PQ16 core inductor
- ER12.7 core inductors / 2 different samples
- ER 25 core inductor

Normally construction of all these low cost high current helical wound planar inductors is same. Therefore the influencing variables are identified from core, coil and complete product. The identified variables are given in table 4.1.

Table 4.1: Identified influencing variables to cause thermal strain during reflow

Core	Coil	Complete product
Exposed surface area	Cross section dimension of conductor	Height
Core volume	Number of turns	---
Top surface of product	Total coil height	---
---	Copper volume	---
---	Area of the coil direct expose to heat	---

The variables given in table 4.1 have been checked and recorded. The data is shown in appendix G

50 products on each inductor model were prepared for the evaluation and following data are measured and recorded.

- Inductance value
- Height of product
- Core winding window

- Height of copper coil
- Gap between core and coil on vertical axis

The reflow profile was set with respect to the recommended reflow profile by JEDEC for surface mount components. The reflow profile was checked and verified with temperature profile reader. The temperature profile reader used is DATAPAQ insight profile tracker.

The sample inductors made are sent through reflow oven with a speed of 65cm/minute. The set temperature profile on reflow machine is as follows.

Table 4.2: The reflow oven zones and set values of temperatures

Zones	Z1	Z2	Z3	Z4	Z5	Z6	Z7	Z8	Z9	Z10
Temperature	100	110	130	150	160	200	300	280	90	50

The real temperature profile is shown in appendix H, which is the output from the profile reader. This illustrates and matches with JEDEC standard temperature profile attached in same appendix A

The inductance variation of selected inductor samples data is attached in appendix. The distribution plots were created to express variation among inductors.

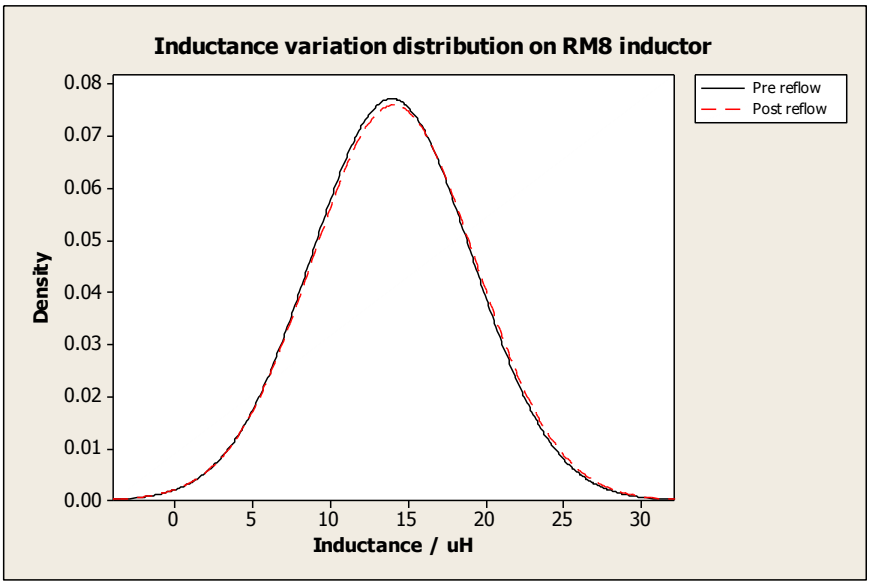

Figure 4.1: Inductance variation distribution curves on RM 8 inductor sample before and after reflow condition.

The figure 4.1 is showing that there is a variation on before and after reflow inductance drop. But the variation is very slight and shows a positive increase in inductance. This can be explainable that the gap is sufficient in the assembled products and the coil deformation on Z direction is not causing any push-ups to make increase gap.

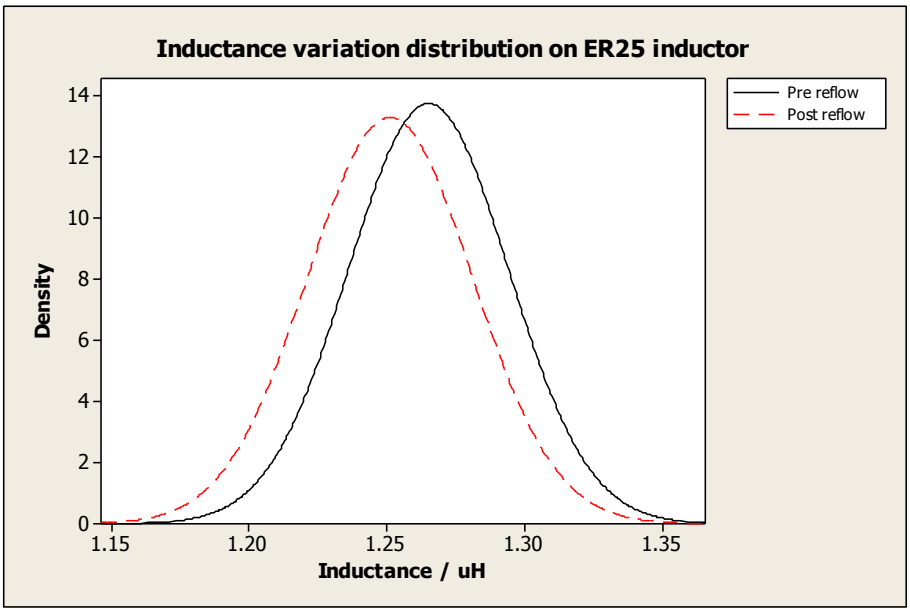

Figure 4.2: Inductance variation distribution curves on ER25 inductor sample before and after reflow condition

The figure 4.2 on ER25 inductor inductance drop is shown very clearly on the plotted distribution curves. The drops in the mean values are shown in appendix E.

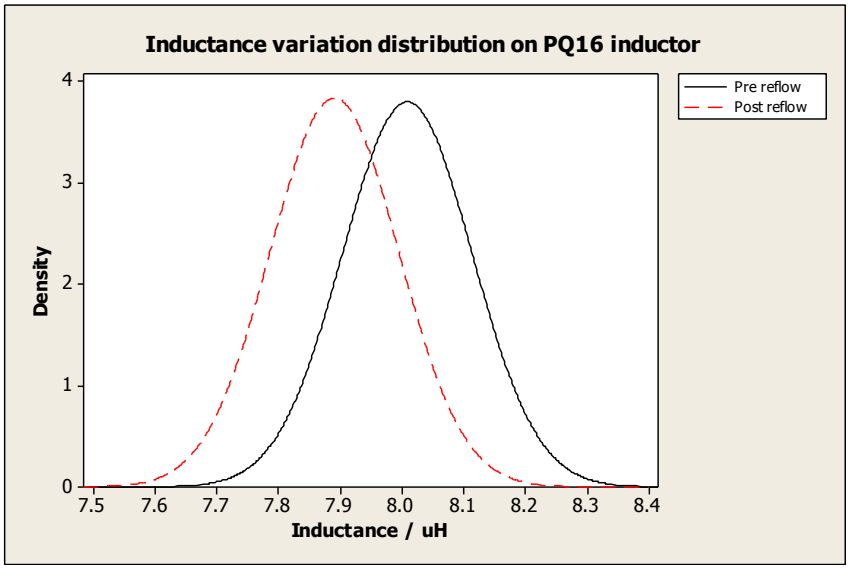

Figure 4.3: Inductance variation distribution curves on PQ16 inductor sample before and after reflow condition

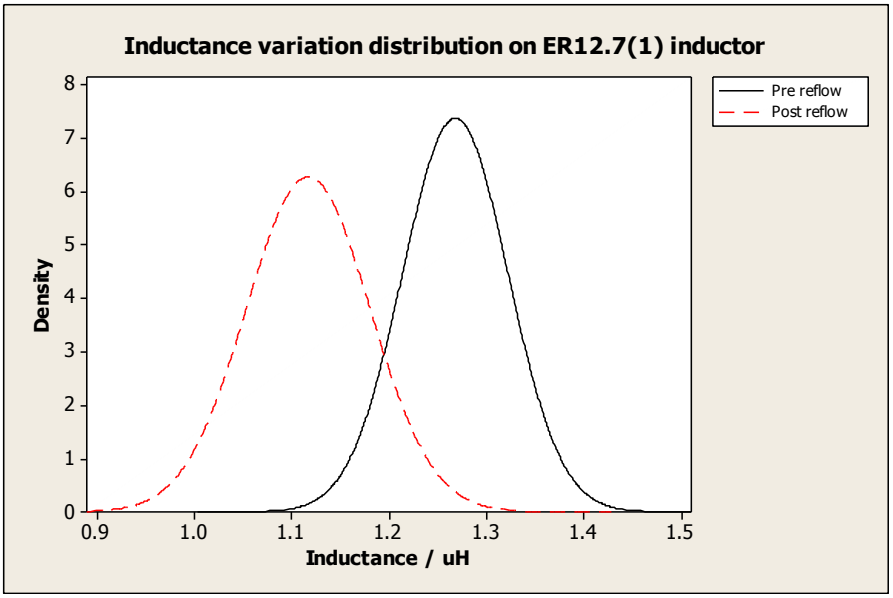

Figure 4.4: Inductance variation distribution curves on ER12.7 model 1 inductor sample before and after reflow condition

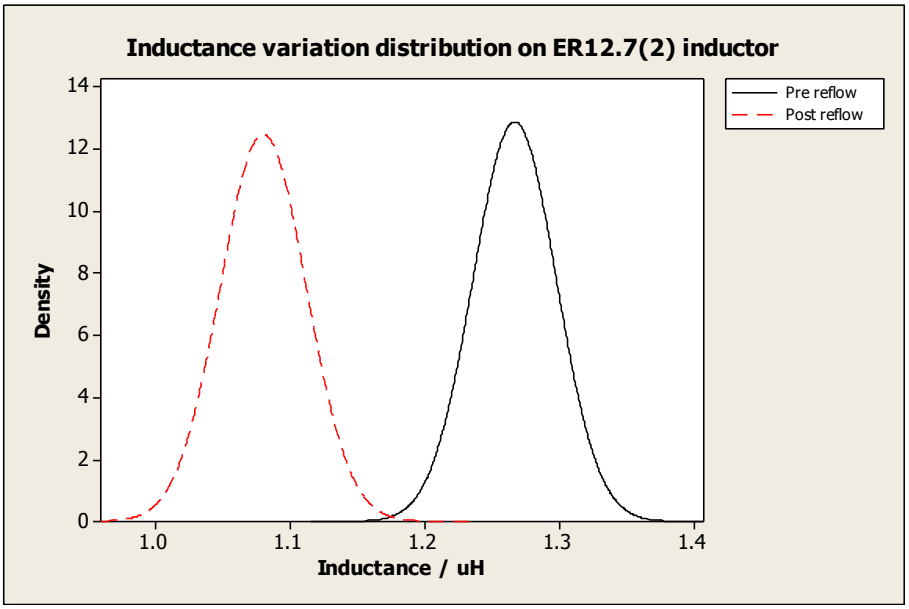

Figure 4.5: Inductance variation distribution curves on ER12.7 model 2 inductor samples before and after reflow condition

The distribution plots are apparently showing variation of inductance on inductors before and after reflow conditions.

The variable parameter influences on inductor models are tabled in table 4.3 as shown below and plotted the variation among inductors.

Table 4.3: The influencing parameter values on respected model inductors

Sample Models	L drop in nH/10	Average Gap*10	core/cu volume ratio	core/cu expose area ratio	Product height/mm	# of turns on back side	Coil height/mm	Conductor thickness/mm	Gap between layers*100
ER25 inductor	1.094	14.920	4.04	8.37	10.48	2	2.75	1.20	35.00
PQ16 inductor	11.554	24.690	2.97	1.97	11.99	10	5.32	0.45	9.11
ER12.7 inductor(1)	13.890	2.888	2.86	13.01	5.86	4	2.58	0.53	15.30
RM8 inductor	16.868	7.886	3.28	1.03	13.65	10	6.81	0.60	9.00
ER12.7 inductor(2)	18.400	3.728	4.26	12.83	5.03	3	1.63	0.40	21.50

The variable parameters were analyzed and the number of turns and the coil height parameters were omitted as the copper volume and the gap between coil and upper cores inner surface are considered.

Influences of the individual parameter were checked along with inductance drop in an increasing manner. The variations were plotted with linear trend lines.

The variations were plotted in the follwing order.

1. ER 25 inductor
2. PQ16 inductor
3. ER12.7 inductor (1)
4. RM8 inductor
5. ER12.7 inductor (2)

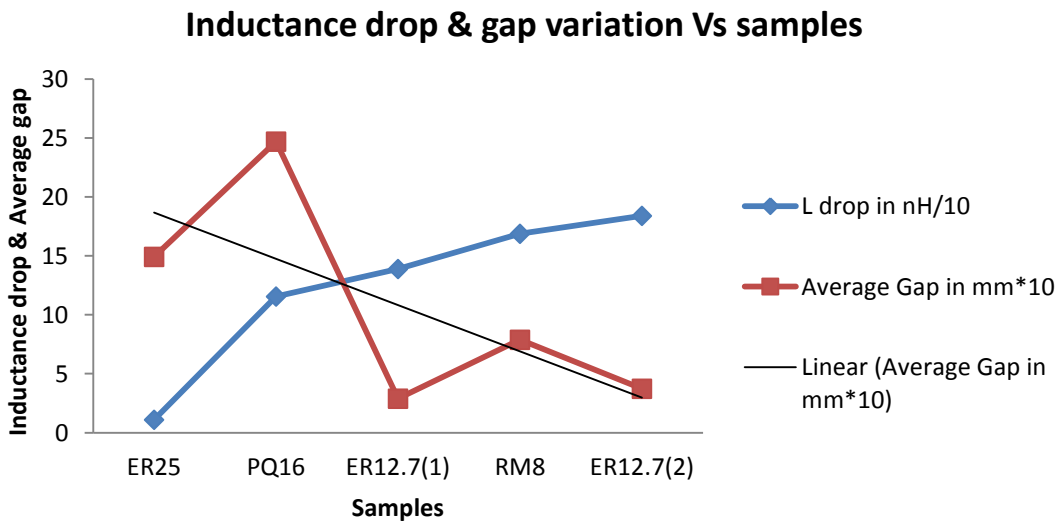

Figure 4.6: The graph of inductance drop and gap variation Vs samples

The inductance drop of selected samples after reflow with respect to average gap was plotted as shown in figure 4.6. The measured inductance drop has been divided by 10 and the gap is multiplied by 10 in order to visually see the trend. The plotted trend line shows a downward trend as the inductance drop is increasing when the gap is reduced. The relationship can be shown as in following format,

Let inductance drop be, L_{drop}

The average gap between coil and upper core inner surface be γ

$$L_{\text{drop}} \alpha\ 1/\gamma \tag{17}$$

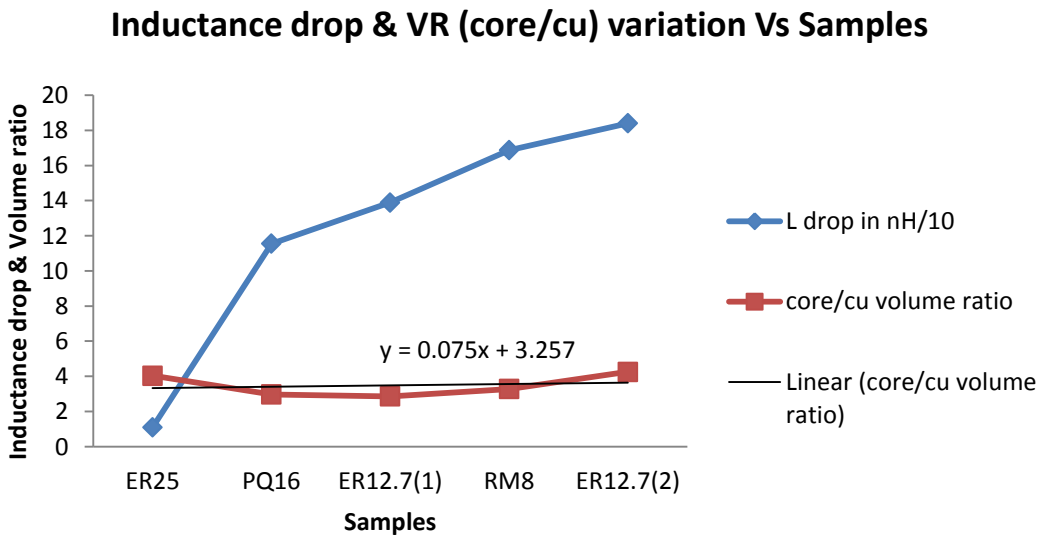

Figure 4.7: The graph of inductance drop and volume ratio of core to copper Vs samples

In graph 4.7, the core to copper volume ratio and inductance drop were plotted against the samples prepared. This graph is illustrating that the inductance drop in increasing when the ferrite core to copper volume ratio increases. It means that when the core volume is high, it can absorbed the heat and dissipates slowly as specific heat capacity of ferrite core is higher than copper. This gives a relationship as following,

Let the volume ratio of ferrite core to copper be $VR_{(\text{core/cu})}$

$$L_{\text{drop}}\ \alpha\ VR_{(\text{core/cu})} \tag{18}$$

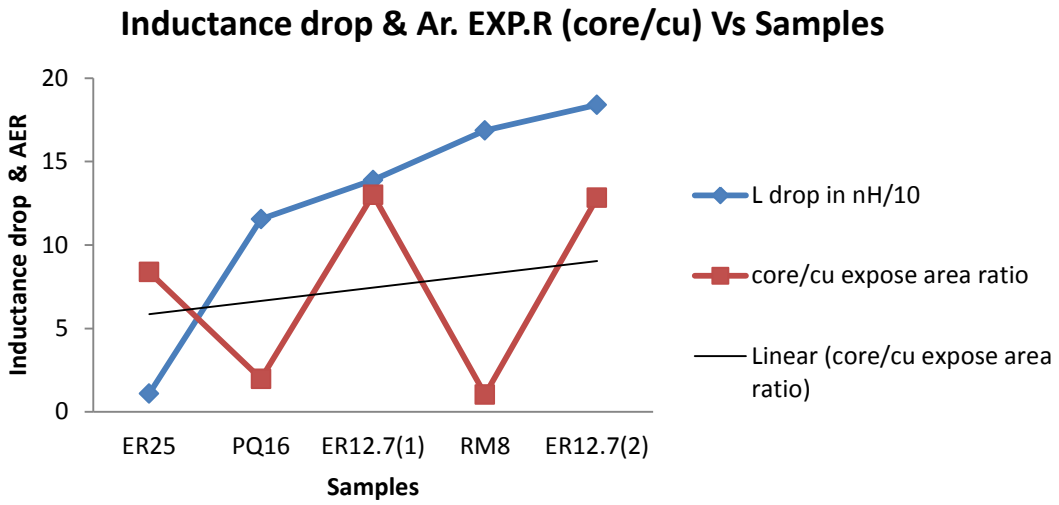

Figure 4.8: The graph of inductance drop and area expose ratio of core to copper Vs samples

In figure 4.8, the relationship between area expose on ferrite core and copper conductor was also considered and the ratio between core and copper was calculated and plotted along with inductance drop against samples. The variation shows like a sea saw pattern with respect to inductance drop in an increasing manner. But the over role trend line shows an increasing line with positive gradient. Therefore the relationship can be summarized as following.

Let the area expose ration between core to copper as $AER_{(\text{core/cu})}$

$$L_{\text{drop}} \; \alpha \; AER_{(\text{core/cu})} \tag{19}$$

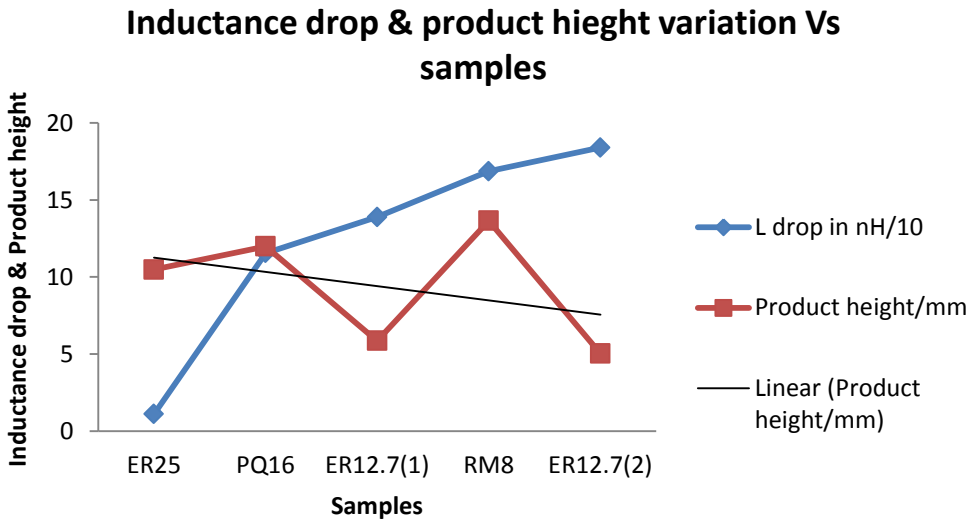

Figure 4.9: The graph of inductance drop and product height variation Vs samples

The product height variation has influenced a lot as this is having an effect during reflow simulation due to different convectional heat transfer co efficient for different height products as per figure 2.3. As shown in figure 4.9, the product height varies along with inductance drop in an increasing manner. But it clearly shows a downward trend line. Therefore the relationship can be obtained as following.

Let the height of the product be H

Hence,

$$L_{drop} \; \alpha \; 1/H \qquad (20)$$

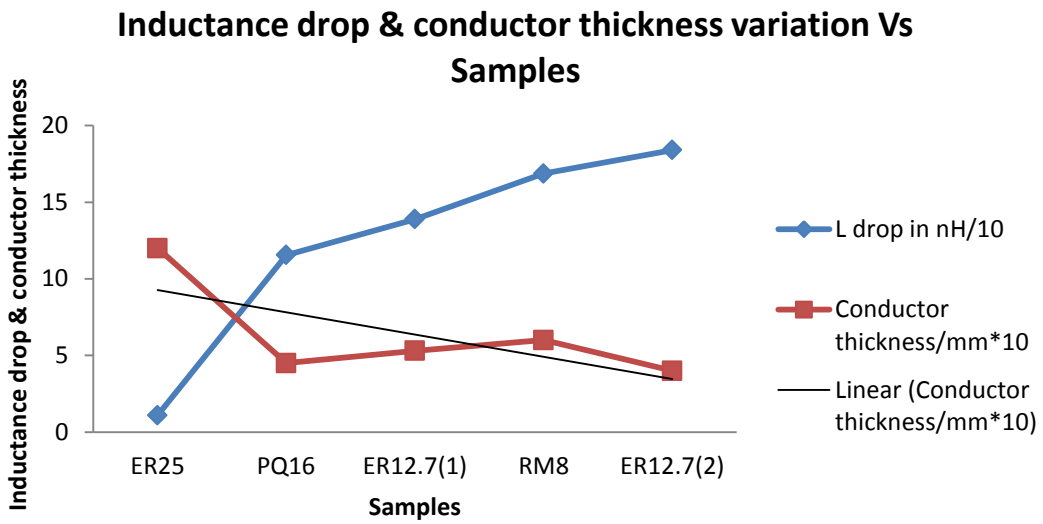

Figure 4.10: The graph of inductance drop and conductor thickness variation Vs samples

The figure 4.10 shows the influence of conductor thickness along with inductance drop on selected samples. It is observed, that the samples having lower conductor thickness shows highest inductance drop. When the conductor thickness is less, it can expand quickly along Z axis (vertical axis), when thermal load is applied on product. The relationship can be derived as following, with respect to plotted trend line.

Let the conductor thickness be *t*,

$$L_{\text{drop}} \, \alpha \, 1/t \tag{21}$$

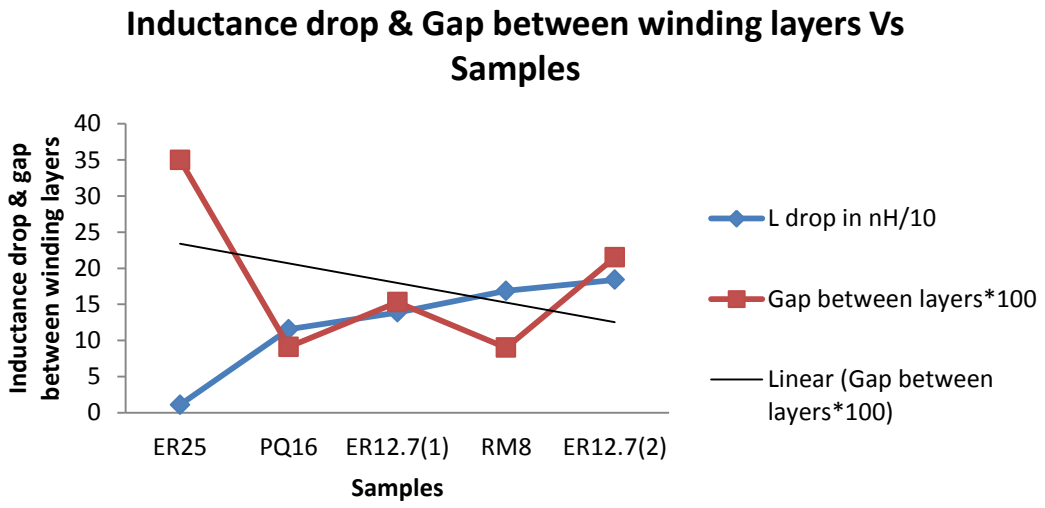

Figure 4.11: The graph of inductance drop and gap between layers Vs samples

The gap between winding layers can eventually reduce gap between core and coil. This tends to easy pushups to drop inductance during reflow. When the gap is high the inductance drop is low, therefore as per trend line outcome, the relationship is derived as following,

Let the winding layer gap be δ,

$$L_{\text{drop}} \; \alpha \; 1/\delta \tag{22}$$

Considering all the above relationships (17), (18), (19), (20), (21) and (22) an iterative equation has formed as in equation (23). The constant K is added to finalize the equation.

$$\boldsymbol{L_{\text{drop}} = K \frac{VR\left(\frac{\text{core}}{\text{cu}}\right).AER\left(\frac{\text{core}}{\text{cu}}\right)}{\gamma.\delta.H.t}} \tag{23}$$

The constant K is calculated as mentioned in table 08, using the equation (23) for different models of inductors.

Table 4.4: The calculated constant (K) values from developed equation

Samples	L drop(nH)	VR	AER	γ	H	t	δ	Calculated K
ER25	10.94	4.04	8.04	1.49	10.48	1.2	0.350	2.21
PQ16	115.54	2.97	1.97	2.47	11.96	0.45	0.091	23.91
RM8	168.68	3.28	1.03	0.79	13.65	0.6	0.090	29.02
ER12.7 (1)	204.06	4.26	12.83	0.37	5.03	0.4	0.215	0.60
ER12.7 (2)	138.94	2.86	13.01	0.29	5.86	0.53	0.153	0.51

The minimum gap requirement is shown in equation 24

$$\gamma_{\mathbf{min}} = \frac{K_{cal}\left(VR_{\left(\frac{\mathbf{core}}{\mathbf{cu}}\right)}.AER_{\left(\frac{\mathbf{core}}{\mathbf{cu}}\right)}\right)}{L_{\mathbf{drop}}.\delta.H.t} \quad (24)$$

4.1 Validation of developed iterative equation:

ER12.7 another model has been selected to evaluate and validate the iterative equation formed, that can used to calculate inductance drop during reflow soldering process. As before another 50 numbers of samples were prepared for evaluation. The inductance was measured before reflow and the samples were sent through reflow in same profile used for earlier evaluations. Then inductance was measured after reflow and recorded. The measured data is attached in appendix I.

Then the developed iterative equation was used to calculate the approximate inductance drop. The calculated constant value (K) on ER12.7 was used to calculate inductance drop with equation. The calculation made is shown in appendix I. A scatter plot with moving average trend line was created to see the variation. As per figure 4.12, the graph shows that the moving average trend line of real inductance drop during reflow simulation is less than the calculated value. An average of 16% difference is shown between practical reflow simulation and calculated inductance drop. Further distribution curves were plotted in figure 4.13 and 4.14 to illustrate the influence and variation at different occasions.

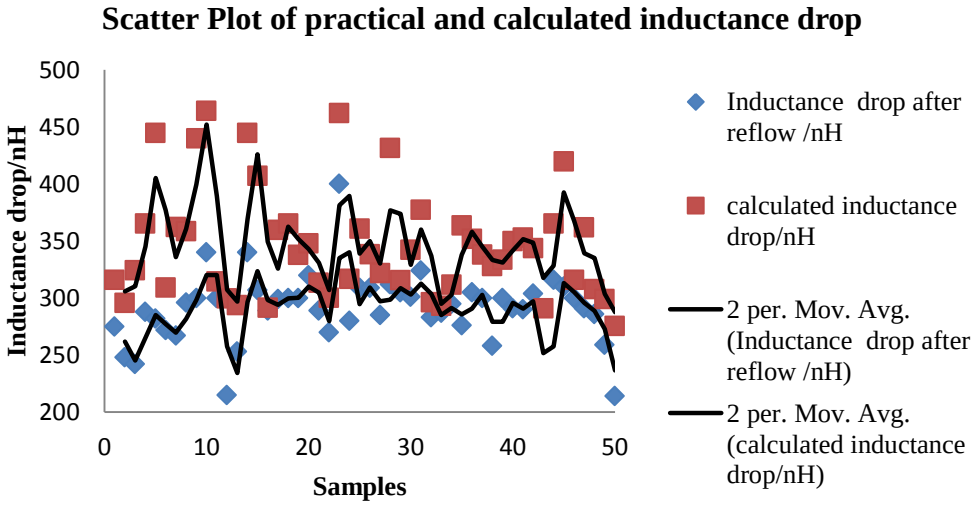

Figure 4.12: The moving average trend line of inductance drop after reflow and calculated drop using developed equation for 50 Nos of ER12.7 model inductor

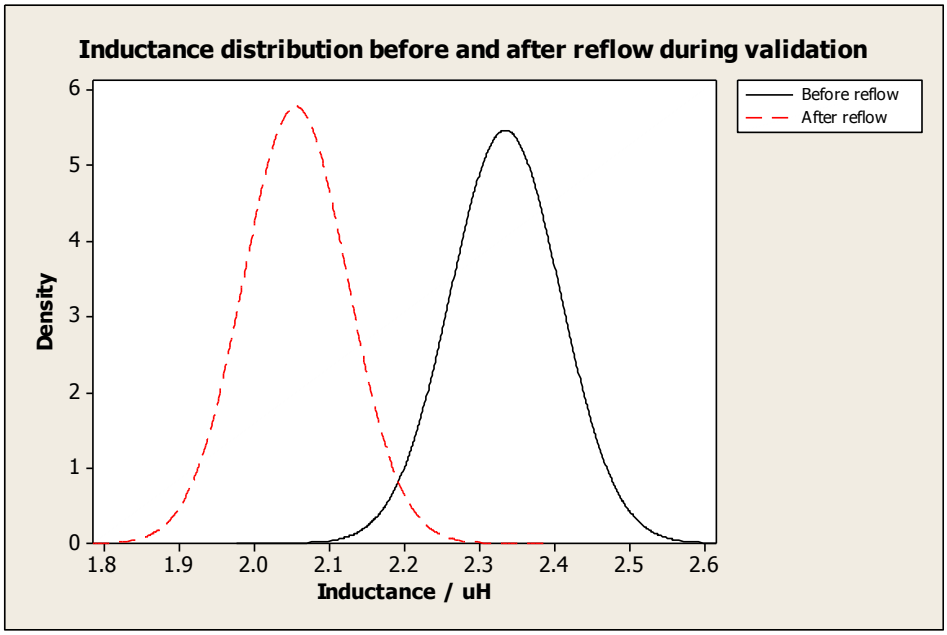

Figure 4.13: The inductance distribution of validation samples before and after reflow

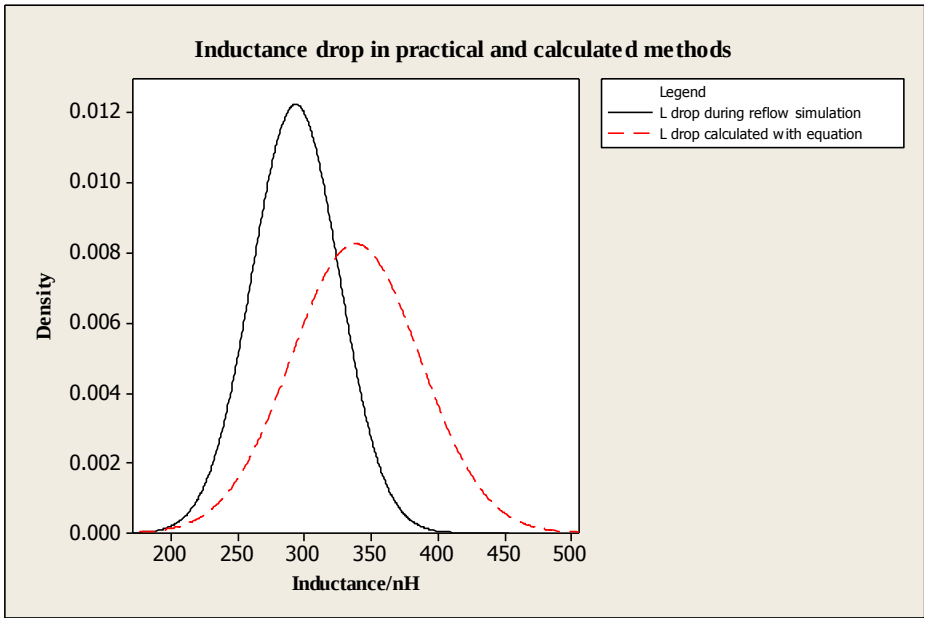

Figure 4.14: The inductance drop in reflow simulation and calculated method using developed equation

The distribution figure 4.14 shows the practical inductance drop is lower than the calculated drop with developed iterative equation. This shows a good indication to use this equation during designing and manufacturing stages to avoid many trial and error methods to solve the problem.

Chapter 5

Conclusion and Recommendation

The equation was formulated with identified most influencing parameters. The reflow soldering oven was mathematically modeled and temperature profile was calculated by following the JEDEC standard for reflow oven soldering process for surface mount devices. The temperature rise was calculated with operational conditions as well and both scenarios are simulated with ANSYS under thermal load. The directional thermal strain was compared and identified that the maximum strain was occurred during reflow oven soldering the product is subjected to thermal load. The directional thermal strain causes in the Z axis. The directional thermal strain causes push up of upper core and causes inductance drop. The influencing parameters were analyzed and formulated the iterative equation. The parameters used are the gap between the copper conductor, volume ratio between ferrite core to copper, area expose ratio between core to copper, complete product height, conductor coil thickness and winding layer gap. All these parameters were analyzed along with inductance drop. The analyses were carried out with five processed power inductor models as ER25, PQ16, two models from ER12.7 and RM8. The inductors were arranged in an order that shows the inductance drop in an increase manner and other parameters were plotted along with inductance drop curve. The relationships were identified with trend line. The volume ratio of core to copper and area expose ratio between core to copper show a proportional relationship to inductance drop and other parameters the gap between conductor and core, product height, conductor thickness and winding layer gap show an inverse proportion to inductance drop.

The formulated equation with most influencing variables was validated by using ER12.7 model. The inductance drops were measured using the same reflow simulation and the inductance drop was calculated by using the developed equation. There is a 16% difference between the calculated inductance drop record and reflow simulation trial. This difference can be minimized by doing the evaluation on different geometry model inductors and same geometry different rating inductors to

make the result of equation further closer to calculated and real reflow simulation inductance drop. The free samples materials from suppliers are very limited and it is hard to expand the evaluation further as well as the cost also high as we need to get materials from abroad. It can be expanded with more models and minimize the difference in inductance drop value in both calculated and during reflow simulation of the formulated equation. This is to be continued as future work.

The main significance of the research is designers of helical wound high current planar power inductor can use the equation during the copper coil thickness and core geometry selection in order to minimize or control the inductance drop in components where a clamp is not used to minimize the total cost of product with the space constrain in printed circuit board. The formulated equation can be used in inductor manufacturing sites to control their core grinding process to avoid the inductance drop at customer end. Eventually the formulated equation will speed up the design and new product introduction (NPI) and avoid time consumption by trial and error method.

The drawback of the work is at least once the profile needs to be verified with the model to calculate the constant value as this can differ with the life time of oven and the efficiency of heaters and blowers. Once the profile is verified that the products are heated up to the JEDEC standard the calculated constant (K) value can be used for other evaluation.

REFERENCES:

1. Eric Coutes.”Practical Inductor,”Internet: www.learnabout-electronics.org/ac_theory/inducto03.php,Sep.04,2013 [Jan.25,2015]
2. Tavarez, A. *et al*, ”Modeling the thermal behavior of solder paste inside reflow ovens,” Journal of Electronic Packages, vol.125 (2003), pp.335-346.
3. Maheney, H. V., “Thermal modelling of the infrared reflow process for solder ball connect (SBC),” *IBMJ Res. Develop.,* vol.37, no.05, (1993), pp.609-619.
4. S. Haddadi.(2007. Oct). “Processed Power Inductors shine at high frequencies,” Power Electronic Technology.[on-line]. 38(1), pp.33-36 Available: www.powerelectronics.com [Dec.1,2013]
5. M. Gerber, J .A. Ferreira, I. W. Hofsajer, and N. Seliger, “A high-density heat-sink-mounted inductor for automotive application,” *IEEE Trans. Ind.Appl*., vol.40, no.4, pp.1031-1038, Jyl/Aug.2004.
6. R. Worbel, N. McNeill, and P. H. Mellor,. ”Performance analysis and thermal modelling of a high-energy-density prebiased inductor,” *IEEE Trans. Ind.Electron*., vol.57, no.1, pp.201-208, Jan.2010.
7. W. G. Odendaal, J.Azevedo, G. W. Brunning, and R. M. Wolf, “A high-efficiency mangentic component with superior calorimetric performance for low-profile high density power conversion.” *IEEE Trans. Ind.Appl*., vol.40, no.5, pp. 1287-1293, Sep./Oct.2004.
8. S. Wang, M. A. de Rooji, W.G. Odendaal, J. D. van Wyk, and D. Boroyevich, “Reduction of high-frequency conduction losses using a planar Litz structure,” *IEEE Trans. Power Electron*., vol. 20, no. 02, pp. 261-267, Mar. 2005.
9. G. L. Skibinski, B. G. Schram, J. R. Brauer, and Z. Badics, “Finite element prediction of losses and temperatures of laminated and composite inductors for AC drives,” in *Proc. IEEE IEMDC*, Jun. 1–4, 2003, pp. 756–763.
10. X. Mao, W. Chen, and Y. Li, “Winding loss mechanism analysis and design for new structure high-frequency gapped inductor,” *IEEE Trans. Magn.*, vol. 41, no. 10, pp. 4036–4038, Oct. 2005.

11. J. Fletcher, B. Williams, and M. Mahmoud, “Airgap fringing flux reduction in inductors using open-circuit copper screens,” *Proc. Inst. Elect. Eng.—Elect. Power Appl.*, vol. 152, no. 4, pp. 990–996, Jul. 2005.
12. K. Nakamura, H. Yoshida, and O. Ichinokura, “Electromagnetic and thermal coupled analysis of ferrite orthogonal-core based on threedimensional reluctance and thermal resistance network model,” *IEEE Trans. Magn.*, vol. 40, no. 4, pp. 2050–2052, Jul. 2004.
13. G. R. Kamath, “An electrical circuit based 3-D thermal model of a fan cooled 600 μH, 80 A inductor for a plasma cutting power supply,” in *Proc. IEEE 23rd Annu. APEC*, Feb. 24–28, 2008, pp. 402–408.
14. R.Wrobel, and.P.H. Mellor, “Thermal design of high-energy density wound components,” *IEEE Trans. Ind.Electron.*, vol.58, no.9, pp.4096-4104, Sep.2011.
15. IPC/JEDEC. “Moisture/Reflow sensitivity classification for nonhermetic solid state surface mount devices,” IPC/JEDEC J-STD-020D.1, March.1, 2008.
16. M. Inoue and T. Koyanagawa. “Thermal simulation for predicting substrate temperature during reflow soldering process,” presented at Electronic Components and Technology Conference, Yokohoma, Japan, 2005.
17. Nakao. H, Hiraizumi. A, and Iwasaki, E., “Reflow oven for a Pb-free Soldering Process,” *Furukawa Review*,” No 20, pp. 77-82, 2001.
17 D.A.Staton and A.Cavagnino,”Convection heat transfer and flow calculations suitable for electric machines thermal models,” *IEEE Trans. Ind.Electron.*, vol.55, no.10, pp.3509-3516, Oct.2008.
18 J.H.Lienhard, “Modes of heat transfer,” in *A heat transfer text book*, 3rd ed, vol 1, J.H.Lienhard, Ed.Cambridge,2003, pp.10-35.
19 Zhuqing Zhang; Sitaraman, S.K.; Wong, C.P., "FEM modeling of temperature distribution of a flip-chip no-flow under fill package during solder reflow process," *Electronics Packaging Manufacturing, IEEE Transactions on* , vol.27, no.1, pp.86-93, Jan. 2004

20 Balazs Illes. Gabor Harsanyi, “3D mapping of forced convection efficiency in reflow ovens, “presented at the Periodic. Polytechnica. Elec. Eng., Vol. 52, No. 1-2, pp. 59-65, (2008).

21 K.L. Lawrence. “Heat transfer and thermal stresses,” in *ANSYS workbench tutorial*, 13 release, K.L. Lawrence, Ed.India:SDC publication,2011,pp.7.1-7.26.

22 Colonel Wm. T. McLyman. “DC inductor design using powder cores,” *in Transformer and inductor design hand book*, 3rd edition, Ed.USA:Library of congress cataloging-in-publication data, 2004, chapter 9.

23 J.Hu, C.R.Sullivan, “AC resistance of planar power inductors ad the quasidistributed gap techniques,” *IEEE Trans. Power.Electron.*, vol.16, no.04, pp.558-567, Jul.2004.

Appendix A

Typical Lead free solder profile for surface mount components

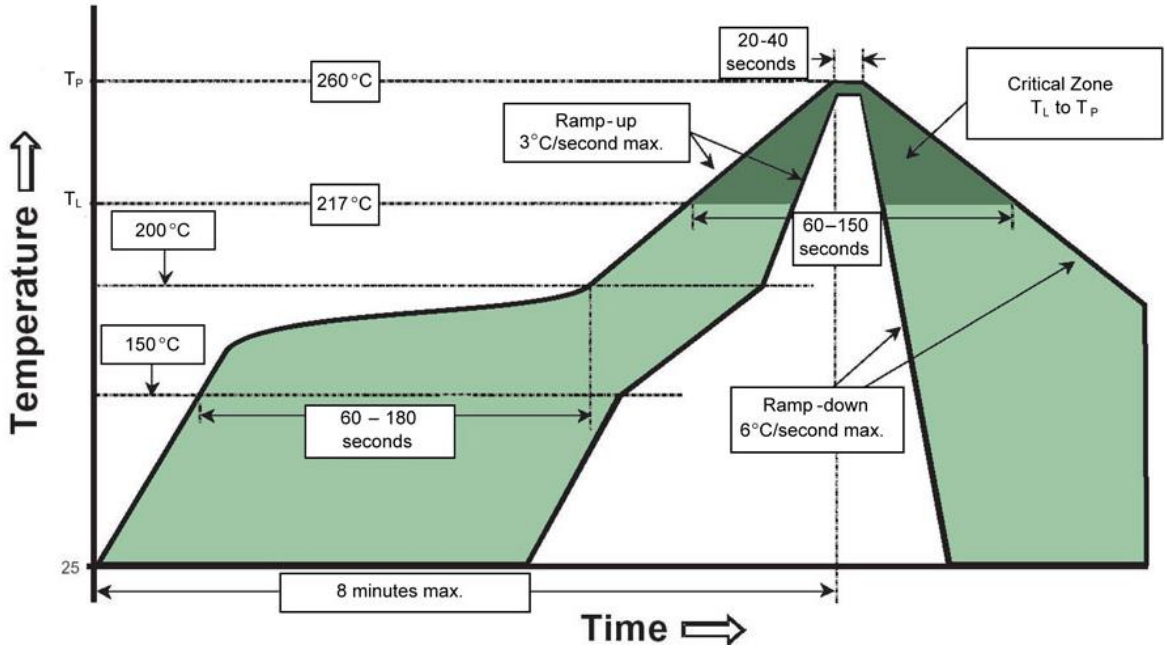

Source: The profile clarification as per IPC/JEDED J-STD-020C Lead free small body assembly

Appendix B
Data collection of ER12.7 (2) model

Sample Model: ER12.7 (2)

No	Sample Height /mm	Inductance Before reflow 100kHz/100mV	Sample Height /mm	Inductance after reflow 100kHz/100mV	L variation	Core window/mm	Cu coil Height/mm	Gap between core and coil/mm
1	4.96	1.300	4.98	1.11	0.190	1.96	1.66	0.30
2	5.01	1.258	5.03	1.07	0.188	2.04	1.67	0.37
3	5.01	1.298	5.00	1.11	0.188	1.97	1.62	0.35
4	5.00	1.233	5.00	1.05	0.183	1.99	1.65	0.34
5	5.01	1.284	5.02	1.09	0.194	2.04	1.65	0.39
6	5.02	1.275	5.04	1.09	0.185	2.00	1.63	0.37
7	5.05	1.278	5.05	1.09	0.188	2.01	1.64	0.37
8	5.11	1.254	5.12	1.07	0.184	2.03	1.60	0.43
9	5.04	1.252	5.03	1.07	0.182	1.96	1.63	0.33
10	5.05	1.305	5.08	1.13	0.175	1.99	1.63	0.36
11	5.02	1.280	5.05	1.10	0.180	1.98	1.63	0.35
12	4.97	1.315	4.97	1.14	0.175	2.00	1.65	0.35
13	5.02	1.301	5.07	1.12	0.181	2.04	1.65	0.39
14	5.12	1.217	5.11	1.04	0.177	1.95	1.66	0.29
15	5.05	1.219	5.05	1.04	0.179	2.01	1.66	0.35
16	4.97	1.285	4.98	1.10	0.185	1.98	1.64	0.34
17	5.09	1.266	5.10	1.09	0.176	1.99	1.63	0.36
18	4.97	1.264	4.99	1.08	0.184	2.03	1.63	0.40
19	5.03	1.280	5.04	1.10	0.180	2.04	1.63	0.41
20	5.03	1.278	5.07	1.10	0.178	2.00	1.62	0.38
21	5.12	1.272	5.10	1.09	0.182	2.05	1.62	0.43
22	5.05	1.240	5.03	1.05	0.190	1.99	1.64	0.35
23	4.97	1.331	5.00	1.14	0.191	1.96	1.63	0.33
24	5.10	1.319	5.11	1.13	0.189	1.98	1.64	0.34
25	5.05	1.274	5.06	1.09	0.184	2.05	1.65	0.40
26	4.95	1.248	5.02	1.06	0.188	2.02	1.65	0.37
27	5.06	1.217	5.03	1.03	0.187	2.02	1.62	0.40
28	5.03	1.255	5.04	1.07	0.185	2.03	1.63	0.40
29	4.92	1.268	4.94	1.08	0.188	1.97	1.62	0.35
30	5.06	1.247	5.07	1.07	0.177	1.98	1.63	0.35
31	4.97	1.259	4.98	1.07	0.189	2.01	1.61	0.40
32	5.03	1.267	5.05	1.08	0.187	1.98	1.61	0.37
33	5.08	1.277	5.08	1.09	0.187	1.99	1.63	0.36
34	4.97	1.325	4.98	1.14	0.185	2.00	1.66	0.34
35	4.95	1.270	4.96	1.08	0.190	1.98	1.65	0.33
36	5.06	1.237	5.06	1.05	0.187	1.99	1.64	0.35
37	4.99	1.260	5.03	1.07	0.190	2.00	1.62	0.38
38	5.09	1.317	5.09	1.13	0.187	1.98	1.58	0.40
39	5.05	1.219	5.06	1.10	0.119	2.01	1.57	0.44
40	5.02	1.354	5.01	1.17	0.184	2.02	1.56	0.46
41	5.00	1.228	5.00	1.04	0.188	2.02	1.61	0.41
42	5.05	1.265	5.07	1.08	0.185	1.96	1.63	0.33
43	5.08	1.262	5.07	1.08	0.182	1.98	1.56	0.42
44	5.05	1.217	5.07	1.07	0.147	2.04	1.57	0.47
45	5.10	1.248	5.11	1.06	0.188	2.04	1.63	0.41
46	4.97	1.256	4.96	1.01	0.246	2.01	1.67	0.34
47	5.02	1.296	5.02	1.11	0.186	2.01	1.62	0.39
48	5.09	1.268	5.09	1.08	0.188	1.99	1.61	0.38
49	4.99	1.261	4.96	1.07	0.191	1.97	1.63	0.34
50	5.10	1.244	5.09	1.06	0.184	1.97	1.60	0.37
Average	**5.03**	**1.269**	**5.04**	**1.08**	**0.184**	**2.00**	**1.63**	**0.37**
Std	**0.050**	**0.031**	**0.046**	**0.032**	**0.015**	**0.027**	**0.026**	**0.038**
median	**5.03**	**1.267**	**5.04**	**1.08**	**0.185**	**2.00**	**1.63**	**0.37**

Appendix C
Data collection of ER12.7 (1) model

ER12.7 (1) sample Model

No	Sample Height /mm	Inductance Before reflow 100kHz/100mV	Sample Height /mm	Inductance after reflow 100kHz/100mV	L variation	Core window/mm	Cu coil Height/mm	Gap between core and coil/mm
1	5.90	1.427	5.89	1.315	0.112	2.83	2.59	0.24
2	5.84	1.386	5.85	1.196	0.190	2.84	2.55	0.29
3	5.82	1.355	5.85	1.255	0.100	2.75	2.53	0.22
4	5.90	1.346	5.91	1.223	0.123	2.94	2.58	0.36
5	5.92	1.377	5.91	1.290	0.087	2.95	2.60	0.35
6	5.93	1.392	5.92	1.268	0.124	2.81	2.60	0.21
7	5.80	1.349	5.82	1.258	0.091	2.76	2.59	0.17
8	5.85	1.358	5.84	1.196	0.162	2.74	2.58	0.16
9	5.83	1.264	5.84	1.125	0.139	2.96	2.58	0.38
10	5.80	1.420	5.8	1.309	0.111	2.94	2.56	0.38
11	5.83	1.333	5.84	1.211	0.122	2.76	2.57	0.19
12	5.84	1.260	5.85	1.112	0.148	2.90	2.58	0.32
13	5.84	1.301	5.85	1.198	0.103	2.95	2.57	0.38
14	5.83	1.217	5.84	1.105	0.112	2.94	2.57	0.37
15	5.85	1.219	5.84	1.108	0.111	2.74	2.60	0.14
16	5.93	1.285	5.92	1.155	0.130	2.81	2.58	0.23
17	5.92	1.266	5.93	1.126	0.140	2.83	2.61	0.22
18	5.91	1.264	5.92	1.143	0.121	2.85	2.63	0.22
19	5.80	1.280	5.81	1.107	0.173	2.84	2.58	0.26
20	5.82	1.278	8.82	1.122	0.156	2.94	2.58	0.36
21	5.86	1.272	5.85	1.154	0.118	2.93	2.57	0.36
22	5.82	1.240	5.83	1.102	0.138	2.79	2.58	0.21
23	5.89	1.331	5.9	1.214	0.117	2.80	2.55	0.25
24	5.87	1.319	5.89	1.198	0.121	2.86	2.60	0.26
25	5.86	1.274	5.87	1.101	0.173	2.86	2.59	0.27
26	5.86	1.248	5.85	1.099	0.149	2.84	2.58	0.26
27	5.91	1.217	5.9	1.102	0.115	2.90	2.57	0.33
28	5.87	1.255	5.86	1.060	0.195	2.94	2.57	0.37
29	5.82	1.268	5.81	1.109	0.159	2.95	2.57	0.38
30	5.87	1.247	5.86	1.112	0.135	2.94	2.56	0.38
31	5.86	1.259	5.86	1.104	0.155	2.89	2.57	0.32
32	5.89	1.267	5.88	1.102	0.165	2.87	2.57	0.30
33	5.82	1.277	5.81	1.125	0.152	2.89	2.57	0.32
34	5.83	1.325	5.82	1.198	0.127	2.88	2.55	0.33
35	5.86	1.270	5.84	1.105	0.165	2.89	2.57	0.32
36	5.86	1.237	5.85	1.108	0.129	2.85	2.59	0.26
37	5.83	1.260	5.81	1.109	0.151	2.86	2.60	0.26
38	5.89	1.317	5.88	1.176	0.141	2.89	2.58	0.31
39	5.92	1.219	5.89	1.104	0.115	2.87	2.56	0.31
40	5.93	1.354	5.91	1.169	0.185	2.88	2.57	0.31
41	5.94	1.228	5.92	1.105	0.123	2.86	2.58	0.28
42	5.95	1.265	5.93	1.123	0.142	2.84	2.57	0.27
43	5.83	1.262	5.82	1.104	0.158	2.87	2.56	0.31
44	5.86	1.217	5.85	1.076	0.141	2.89	2.57	0.32
45	5.82	1.248	5.83	1.112	0.136	2.88	2.59	0.29
46	5.86	1.256	5.84	1.090	0.166	2.86	2.62	0.24
47	5.90	1.296	5.88	1.125	0.171	2.95	2.61	0.34
48	5.83	1.268	5.82	1.112	0.156	2.93	2.58	0.35
49	5.85	1.261	5.83	1.105	0.156	2.81	2.59	0.22
50	5.86	1.244	5.82	1.106	0.138	2.83	2.57	0.26
Average	**5.86**	**1.288**	**5.92**	**1.149**	**0.139**	**2.87**	**2.58**	**0.29**
Std	**0.0405**	**0.0541**	**0.4202**	**0.0636**	**0.0252**	**0.0603**	**0.0185**	**0.0638**
median	**5.86**	**1.268**	**5.85**	**1.117**	**0.139**	**2.87**	**2.58**	**0.30**

Appendix D
Data collection of RM8 model

RM8 Sample Model								
No	H/mm	Inductance Before reflow 100kHz/100mV	H/mm	Inductance after reflow 100kHz/100mV	L variation	Core window/ mm	Cu coil Height/m m	Gap between core and coil/mm
1	13.64	13.950	13.66	14.016	0.066	7.64	6.63	1.01
2	13.64	13.752	13.85	14.110	0.358	7.63	6.75	0.88
3	13.63	24.826	13.65	24.849	0.023	7.61	6.72	0.89
4	13.64	15.360	13.63	15.446	0.086	7.62	6.77	0.85
5	13.57	21.380	13.58	21.629	0.249	7.68	6.97	0.71
6	13.55	14.216	13.84	14.359	0.143	7.51	6.76	0.75
7	13.69	13.876	13.70	14.009	0.133	7.60	7.17	0.43
8	13.67	14.282	13.70	14.409	0.127	7.56	6.79	0.77
9	13.66	14.107	13.65	14.256	0.149	7.55	6.67	0.88
10	13.67	13.926	13.70	14.004	0.078	7.61	6.71	0.90
11	13.64	13.827	13.77	13.960	0.133	7.66	6.86	0.80
12	13.65	13.619	13.67	13.704	0.085	7.50	6.78	0.72
13	13.66	13.882	13.74	14.050	0.168	7.64	6.85	0.79
14	13.74	13.936	13.86	14.066	0.130	7.62	6.68	0.94
15	13.74	13.689	13.75	13.866	0.177	7.51	7.08	0.43
16	13.72	13.779	13.72	13.895	0.116	7.50	6.97	0.53
17	13.60	13.624	13.84	13.785	0.161	7.64	6.83	0.81
18	13.68	14.032	13.72	14.159	0.127	7.60	6.85	0.75
19	13.60	13.893	13.74	14.029	0.136	7.57	6.75	0.82
20	13.81	13.958	13.67	14.091	0.133	7.52	6.87	0.65
21	13.70	14.077	13.73	14.250	0.173	7.60	6.86	0.74
22	13.57	14.198	13.73	14.395	0.197	7.60	6.68	0.92
23	13.75	14.194	13.85	14.305	0.111	7.68	6.80	0.88
24	13.75	14.055	13.78	14.166	0.111	7.64	6.86	0.78
25	13.70	31.788	13.67	32.859	1.071	7.60	7.00	0.60
26	13.62	14.035	13.77	14.800	0.765	7.69	6.82	0.87
27	13.57	13.881	13.57	13.980	0.099	7.60	6.83	0.77
28	13.62	13.908	13.71	13.966	0.058	7.53	6.75	0.78
29	13.70	13.587	13.69	13.705	0.118	7.54	6.71	0.83
30	13.60	13.664	13.70	13.720	0.056	7.60	6.71	0.89
31	13.64	13.867	13.70	14.039	0.172	7.55	6.77	0.78
32	13.59	13.623	13.65	13.745	0.122	7.50	6.77	0.73
33	13.65	38.158	13.67	38.400	0.242	7.58	6.77	0.81
34	13.62	27.708	13.57	27.950	0.242	7.63	6.71	0.92
35	13.71	12.309	13.73	11.905	-0.404	7.67	6.99	0.68
36	13.71	13.372	13.64	14.156	0.784	7.50	6.80	0.70
37	13.80	13.959	13.87	14.075	0.116	7.53	6.76	0.77
38	13.77	12.287	13.71	12.370	0.083	7.62	7.00	0.62
39	13.59	27.393	13.63	27.650	0.257	7.63	6.67	0.96
40	13.63	16.478	13.68	16.550	0.072	7.56	6.82	0.74
41	13.73	13.957	13.70	14.033	0.076	7.50	6.72	0.78
42	13.63	13.994	13.83	14.080	0.086	7.65	6.72	0.93
43	13.55	14.255	13.83	14.345	0.090	7.63	6.76	0.87
44	13.69	14.013	13.70	14.080	0.067	7.65	6.74	0.91
45	13.62	14.224	13.65	14.307	0.083	7.65	6.77	0.88
46	13.72	14.017	13.66	14.150	0.133	7.65	6.77	0.88
47	13.60	13.953	13.63	14.035	0.082	7.55	6.85	0.70
48	13.72	14.146	13.70	14.265	0.119	7.67	6.82	0.85
49	13.52	14.180	13.55	14.562	0.382	7.67	6.70	0.97
50	13.52	13.722	13.54	13.815	0.093	7.47	6.89	0.58
Average	**13.66**	**15.698**	**13.71**	**15.867**	**0.169**	**7.59**	**6.81**	**0.79**
Std	**0.069**	**5.171**	**0.082**	**5.252**	**0.210**	**0.060**	**0.110**	**0.128**
median	**13.65**	**13.959**	**13.7**	**14.086**	**0.125**	**7.60**	**6.77**	**0.80**

Appendix E
Data collection of ER25 model

ER25 inductor sample model

No	H/mm	Inductance Before reflow 100kHz/100mV	H/mm	Inductance after reflow 100kHz/100mV	L variation	Core window/mm	Cu coil Height/mm	Gap between core and coil/mm
1	10.49	1.221	10.49	1.209	0.012	4.25	2.74	1.51
2	10.45	1.264	10.43	1.250	0.014	4.17	2.88	1.29
3	10.46	1.278	10.43	1.220	0.058	4.34	2.73	1.61
4	10.45	1.210	10.46	1.201	0.009	4.24	2.84	1.40
5	10.55	1.283	10.47	1.270	0.013	4.13	2.73	1.40
6	10.40	1.320	10.40	1.310	0.010	4.22	2.78	1.44
7	10.48	1.266	10.52	1.213	0.053	4.29	2.72	1.57
8	10.63	1.268	10.63	1.247	0.021	4.14	2.78	1.36
9	10.35	1.278	10.35	1.270	0.008	4.22	2.71	1.51
10	10.46	1.330	10.45	1.326	0.004	4.17	2.81	1.36
11	10.44	1.247	10.45	1.240	0.007	4.19	2.90	1.29
12	10.43	1.249	10.50	1.249	0.000	4.21	2.78	1.43
13	10.51	1.269	10.50	1.269	0.000	4.28	2.77	1.51
14	10.53	1.225	10.60	1.223	0.002	4.32	2.80	1.52
15	10.58	1.245	10.61	1.243	0.002	4.31	2.74	1.57
16	10.57	1.220	10.50	1.222	-0.002	4.26	2.67	1.59
17	10.47	1.305	10.51	1.299	0.006	4.27	2.84	1.43
18	10.49	1.244	10.47	1.230	0.014	4.15	2.73	1.42
19	10.45	1.297	10.45	1.279	0.018	4.16	2.78	1.38
20	10.44	1.266	10.69	1.253	0.013	4.18	2.72	1.46
21	10.48	1.269	10.46	1.260	0.009	4.19	2.69	1.50
22	10.48	1.271	10.55	1.263	0.008	4.25	2.75	1.50
23	10.47	1.254	10.52	1.241	0.013	4.24	2.76	1.48
24	10.45	1.280	10.45	1.275	0.005	4.23	2.80	1.43
25	10.46	1.309	10.48	1.304	0.005	4.28	2.79	1.49
26	10.46	1.278	10.47	1.270	0.008	4.27	2.66	1.61
27	10.50	1.261	10.50	1.256	0.005	4.29	2.68	1.61
28	10.52	1.230	10.55	1.219	0.011	4.34	2.73	1.61
29	10.45	1.260	10.50	1.254	0.006	4.33	2.84	1.49
30	10.60	1.277	10.61	1.270	0.007	4.32	2.73	1.59
31	10.52	1.233	10.52	1.219	0.014	4.21	2.69	1.52
32	10.46	1.300	10.45	1.228	0.072	4.22	2.74	1.48
33	10.56	1.255	10.46	1.324	-0.069	4.23	2.68	1.55
34	10.46	1.280	10.52	1.265	0.015	4.28	2.78	1.50
35	10.54	1.235	10.55	1.243	-0.008	4.29	2.78	1.51
36	10.45	1.279	10.48	1.270	0.009	4.35	2.72	1.63
37	10.50	1.233	10.56	1.223	0.010	4.32	2.75	1.57
38	10.48	1.328	10.56	1.225	0.103	4.36	2.72	1.64
39	10.37	1.260	10.37	1.250	0.010	4.38	2.71	1.67
40	10.44	1.313	10.45	1.309	0.004	4.35	2.81	1.54
41	10.44	1.276	10.45	1.270	0.006	4.15	2.80	1.35
42	10.33	1.260	10.39	1.251	0.009	4.29	2.77	1.52
43	10.34	1.233	10.37	1.226	0.007	4.16	2.84	1.32
44	10.53	1.264	10.55	1.260	0.004	4.18	2.73	1.45
45	10.45	1.246	10.42	1.241	0.005	4.19	2.78	1.41
46	10.51	1.258	10.51	1.250	0.008	4.23	2.72	1.51
47	10.52	1.238	10.58	1.238	0.000	4.21	2.79	1.42
48	10.47	1.224	10.55	1.226	-0.002	4.22	2.78	1.44
49	10.45	1.292	10.43	1.288	0.004	4.28	2.69	1.59
50	10.42	1.273	10.41	1.266	0.007	4.33	2.67	1.66
Average	**10.47**	**1.265**	**10.49**	**1.254**	**0.011**	**4.25**	**2.76**	**1.49**
Std	**0.06**	**0.029**	**0.07**	**0.030**	**0.022**	**0.07**	**0.05**	**0.10**
median	**10.47**	**1.265**	**10.49**	**1.251**	**0.008**	**4.25**	**2.75**	**1.50**

Appendix F
Data collection of PQ16 model

PQ16 inductor sample model

No	H/mm	Inductance Before reflow 100kHz/100mV	H/mm	Inductance after reflow 100kHz/100mV	L variation	Core window/mm	Cu coil Height/mm	Gap between core and coil/mm
1	12.01	7.926	11.98	7.859	0.067	7.80	5.59	2.21
2	12.00	8.110	12.01	8.059	0.051	7.83	5.40	2.43
3	11.98	8.162	12.01	8.071	0.091	7.75	5.39	2.36
4	12.01	8.042	12.01	7.976	0.066	7.88	5.35	2.53
5	12.01	8.142	11.99	8.099	0.043	7.93	5.60	2.33
6	11.98	7.913	11.98	7.817	0.096	7.70	5.45	2.25
7	12.00	8.015	12.01	7.934	0.081	7.90	5.42	2.48
8	11.98	8.019	11.98	7.930	0.089	7.83	5.39	2.44
9	11.98	7.849	11.99	7.830	0.019	7.79	5.45	2.34
10	11.99	8.002	11.99	7.923	0.079	7.89	5.36	2.53
11	12.00	7.947	12.00	7.886	0.061	7.72	5.39	2.33
12	12.00	8.100	12.00	8.010	0.090	7.68	5.43	2.25
13	12.00	7.968	12.01	7.872	0.096	7.71	5.70	2.01
14	12.00	7.895	11.99	7.763	0.132	7.90	5.37	2.53
15	11.99	7.989	12.02	7.872	0.117	7.81	5.35	2.46
16	11.99	8.075	11.99	7.972	0.103	7.82	5.23	2.59
17	12.03	7.950	11.98	7.852	0.098	7.83	5.34	2.49
18	11.98	7.866	11.98	7.764	0.102	7.63	5.32	2.31
19	12.00	8.055	11.99	7.937	0.118	7.98	5.20	2.78
20	11.99	8.007	11.99	7.878	0.129	7.71	5.19	2.52
21	12.01	8.090	11.99	7.980	0.110	7.74	5.20	2.54
22	12.01	8.010	12.01	7.907	0.103	7.81	5.25	2.56
23	12.00	7.918	11.98	7.789	0.129	7.87	5.19	2.68
24	11.99	7.976	11.99	7.800	0.176	7.84	5.18	2.66
25	12.00	7.899	11.99	7.863	0.036	7.55	5.16	2.39
26	11.99	8.095	11.98	8.042	0.053	7.71	5.40	2.31
27	11.99	8.168	11.99	8.102	0.066	7.63	5.18	2.45
28	11.99	8.040	11.99	8.000	0.040	7.87	5.20	2.67
29	11.98	7.918	11.99	7.835	0.083	7.68	5.36	2.32
30	12.01	7.910	11.99	7.886	0.024	7.83	5.28	2.55
31	12.00	7.932	11.99	7.875	0.057	7.82	5.30	2.52
32	11.99	7.914	11.99	7.812	0.102	7.79	5.33	2.46
33	11.99	7.994	12.00	7.841	0.153	7.92	5.29	2.63
34	11.99	8.173	11.99	7.999	0.174	7.71	5.26	2.45
35	11.98	7.958	11.99	7.812	0.146	7.82	5.12	2.70
36	11.88	8.032	11.84	7.914	0.118	7.74	5.21	2.53
37	12.00	8.145	11.99	7.966	0.179	7.67	5.34	2.33
38	11.98	8.064	11.48	7.884	0.180	7.77	5.19	2.58
39	12.06	8.145	12.03	7.955	0.190	7.81	5.22	2.59
40	11.99	7.982	11.98	7.831	0.151	7.60	5.17	2.43
41	12.00	8.065	11.99	7.945	0.120	7.77	5.10	2.67
42	12.00	8.161	12.00	8.027	0.134	7.84	5.25	2.59
43	12.00	7.969	12.00	7.809	0.160	7.83	5.38	2.45
44	12.01	8.034	12.04	7.895	0.139	7.74	5.53	2.21
45	12.02	7.980	11.99	7.723	0.257	7.78	5.24	2.54
46	11.99	7.920	11.99	7.637	0.283	7.71	5.26	2.45
47	12.01	8.228	12.00	8.018	0.210	7.73	5.23	2.50
48	12.01	8.354	12.00	8.140	0.214	7.85	5.24	2.61
49	12.04	8.090	12.01	7.915	0.175	7.82	5.23	2.59
50	11.99	7.875	12.02	7.788	0.087	7.70	5.38	2.32
Average	**12.00**	**8.021**	**11.98**	**7.906**	**0.116**	**7.78**	**5.31**	**2.47**
Std	**0.02**	**0.105**	**0.08**	**0.104**	**0.058**	**0.09**	**0.13**	**0.15**
median	**12.00**	**8.009**	**11.99**	**7.891**	**0.103**	**7.80**	**5.30**	**2.49**

Appendix G
Data collection of all sample models to check parameter influences on inductance drop

Description	PQ16 Sample Inductor		RM8 Sample Inductor		ER12.7(2) Sample Inductor		ER25 Sample Inductor		ER12.7 (1) Inductor Sample		ER12.7 Validation Inductor	
	Cu weight/(g)	Core weight / (g)	Cu weight/(g)	Core weight / (g)	Cu weight/(g)	Core weight / (g)	Cu weight/(g)	Core weight / (g)	Cu weight/(g)	Core weight / (g)	Cu weight/(g)	Core weight / (g)
Average	3.6475	5.810625	5.88	10.35818182	0.77625	1.774166667	7.0675	15.33285714	1.187142857	1.82	1.178888889	2.02
Average weight / (kg)	0.0036475	0.005810625	0.00588	0.010358182	0.00077625	0.001774167	0.0070675	0.015332857	0.001187143	0.00182	0.001178889	0.00202
Density in Kg/m3	8940	4800	8940	4800	8940	4800	8940	4800	8940	4800	8940	4800
Volume/m3	4.07998E-07	1.21055E-06	6.57718E-07	2.15795E-06	8.68289E-08	3.69618E-07	7.90548E-07	3.19435E-06	1.3279E-07	3.79167E-07	1.31867E-07	4.20833E-07
Volume / mm3	407.9977629	1210.546875	657.7181208	2157.954545	86.82885906	369.6180556	790.5480984	3194.345238	132.7900288	379.1666667	131.8667661	420.8333333
Exposed surface area/mm2		605.12		456.65		227.415		1039.52		250		252
Core volume/mm3		1210.546875		2157.954545		369.6180556		3194.345238		379.1666667		420.8333333
Are of top surface/mm2		183.68		273		122.075		500		126.5		126
Coil Width/mm	2.8		2.8		2.2		5.1		2.2			2.2
Coil thickness/mm	0.45		0.6		0.4		1.2		0.53			0.45
Number of turns / nos	9.75		9.75		2.75		1.75		3.75			4.75
Total coil height/mm	5.3118		6.8056		1.627		2.7566		2.578			2.6858
Cu volume/mm3	407.9977629		657.7181208		86.82885906		790.5480984		132.7900288			420.8333333
Coil expose area to heat/mm2	307.23		442.02		17.72		124.17		19.21			18.92
cu/core volume ratio	0.34		0.30		0.23		0.25					
cu/core area expose ratio	0.51		0.97		0.08		0.12					
Core/cu volume ratio	2.97		3.28		4.26		4.04			2.86		3.19
Core/cu area expose ratio	1.97		1.03		12.83		8.37			13.01		13.32

Appendix H
The obtained reflow profile using DATAPAQ profile reader

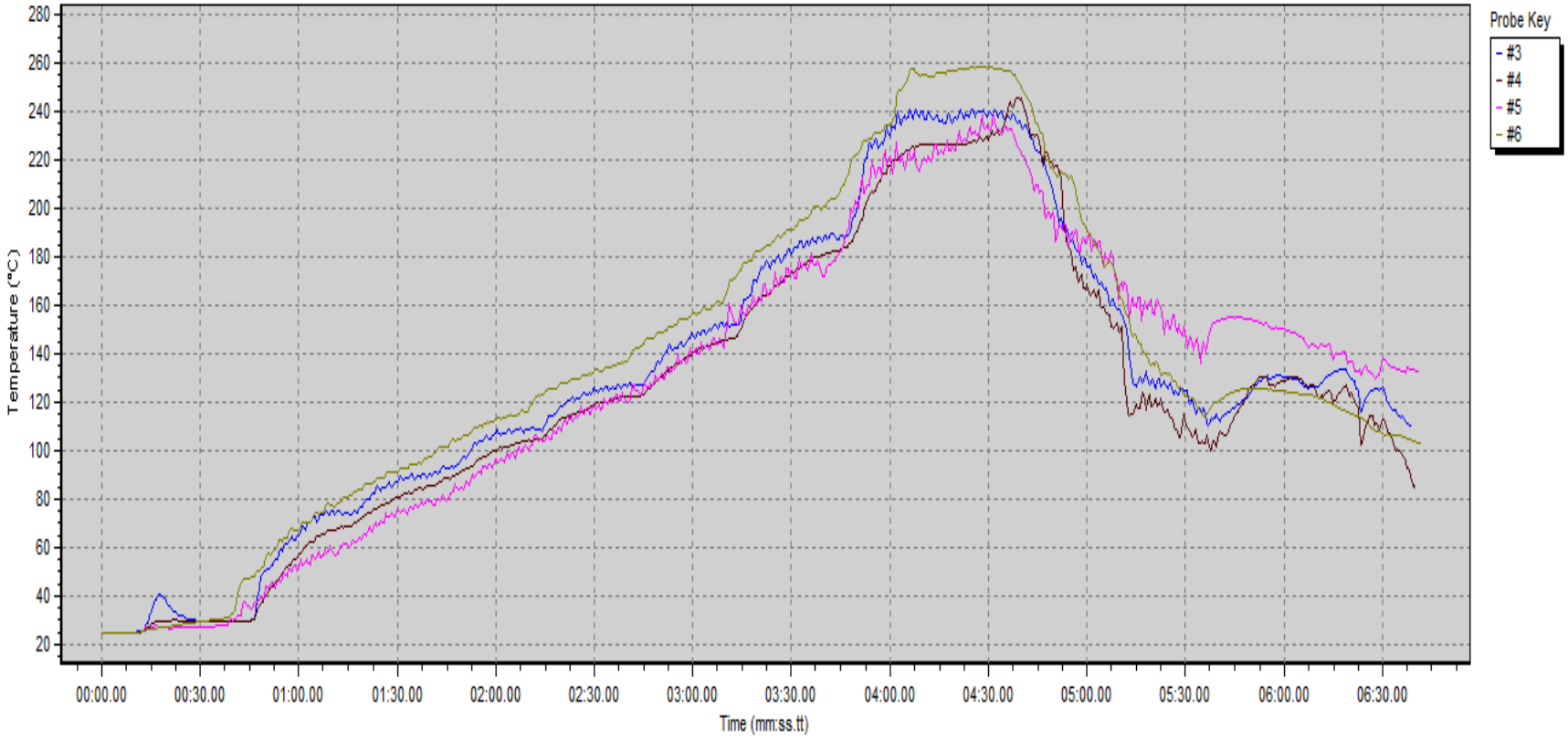

Appendix I

Real and calculated inductance drop of sample model of validation

No	Sample Height/mm	Inductance before reflow uH (100kHz/100mV)	Inductance after reflow uH (100kHz/100mV)	Inductance variations in nH	calculated Ldrop/nH	Core window/ mm	Copper coil height/mm	Gap between core and coil / mm	Average VR	Average AER	conductor thickness t/mm	Winding layer gap delta/mm	Constant K	No of turns on backside	Percentage deviation from calculated value
1	5.99	2.381	2.106	275	316	2.94	2.68	0.26	3.19	13.32	0.45	0.108	0.56	5	13%
2	5.96	2.403	2.155	248	296	2.95	2.65	0.30	3.19	13.32	0.45	0.100	0.56	5	16%
3	5.97	2.345	2.103	242	324	2.92	2.64	0.28	3.19	13.32	0.45	0.098	0.56	5	25%
4	5.86	2.328	2.040	288	365	2.89	2.63	0.26	3.19	13.32	0.45	0.095	0.56	5	21%
5	5.87	2.374	2.092	282	445	2.82	2.55	0.27	3.19	13.32	0.45	0.075	0.56	5	37%
6	5.89	2.422	2.150	272	309	2.95	2.68	0.27	3.19	13.32	0.45	0.108	0.56	5	12%
7	5.90	2.333	2.066	267	362	2.92	2.70	0.22	3.19	13.32	0.45	0.113	0.56	5	26%
8	5.85	2.257	1.961	296	359	2.94	2.73	0.21	3.19	13.32	0.45	0.120	0.56	5	17%
9	5.87	2.384	2.084	300	440	2.85	2.64	0.21	3.19	13.32	0.45	0.098	0.56	5	32%
10	5.89	2.363	2.023	340	464	2.86	2.68	0.18	3.19	13.32	0.45	0.108	0.56	5	27%
11	5.90	2.325	2.025	300	314	2.93	2.63	0.30	3.19	13.32	0.45	0.095	0.56	5	5%
12	5.88	2.315	2.100	215	300	2.95	2.65	0.30	3.19	13.32	0.45	0.100	0.56	5	28%
13	5.89	2.341	2.088	253	294	2.98	2.72	0.26	3.19	13.32	0.45	0.118	0.56	5	14%
14	5.83	2.320	1.980	340	445	2.90	2.73	0.17	3.19	13.32	0.45	0.120	0.56	5	24%
15	5.89	2.317	2.010	307	407	2.92	2.74	0.18	3.19	13.32	0.45	0.123	0.56	5	25%
16	5.82	2.409	2.120	289	291	2.97	2.68	0.29	3.19	13.32	0.45	0.108	0.56	5	1%
17	5.81	2.497	2.198	299	360	2.92	2.69	0.23	3.19	13.32	0.45	0.110	0.56	5	17%
18	5.85	2.372	2.072	300	365	2.92	2.70	0.22	3.19	13.32	0.45	0.113	0.56	5	18%
19	5.92	2.339	2.039	300	338	2.94	2.71	0.23	3.19	13.32	0.45	0.115	0.56	5	11%
20	5.88	2.355	2.035	320	348	2.94	2.72	0.22	3.19	13.32	0.45	0.118	0.56	5	8%
21	5.86	2.312	2.023	289	313	2.97	2.73	0.24	3.19	13.32	0.45	0.120	0.56	5	8%
22	5.85	2.220	1.950	270	300	2.96	2.68	0.28	3.19	13.32	0.45	0.108	0.56	5	10%
23	5.78	2.608	2.208	400	462	2.87	2.69	0.18	3.19	13.32	0.45	0.110	0.56	5	13%
24	5.89	2.335	2.055	280	317	2.94	2.67	0.27	3.19	13.32	0.45	0.105	0.56	5	12%
25	5.86	2.512	2.203	309	361	2.90	2.65	0.25	3.19	13.32	0.45	0.100	0.56	5	14%
26	5.92	2.279	1.970	309	338	2.93	2.69	0.24	3.19	13.32	0.45	0.110	0.56	5	9%
27	5.84	2.373	2.088	285	322	2.95	2.70	0.25	3.19	13.32	0.45	0.113	0.56	5	11%
28	5.92	2.356	2.044	312	431	2.89	2.71	0.18	3.19	13.32	0.45	0.115	0.56	5	28%
29	5.94	2.295	1.990	305	316	2.96	2.72	0.24	3.19	13.32	0.45	0.118	0.56	5	3%
30	5.85	2.398	2.097	301	342	2.93	2.69	0.24	3.19	13.32	0.45	0.110	0.56	5	12%
31	5.93	2.225	1.901	324	377	2.91	2.70	0.21	3.19	13.32	0.45	0.113	0.56	5	14%
32	5.95	2.338	2.055	283	296	2.95	2.65	0.30	3.19	13.32	0.45	0.100	0.56	5	4%
33	5.93	2.347	2.060	287	293	2.95	2.63	0.32	3.19	13.32	0.45	0.095	0.56	5	2%
34	5.85	2.220	1.925	295	312	2.94	2.65	0.29	3.19	13.32	0.45	0.100	0.56	5	5%
35	5.88	2.321	2.045	276	364	2.91	2.68	0.23	3.19	13.32	0.45	0.108	0.56	5	24%
36	5.94	2.303	1.998	305	352	2.92	2.69	0.23	3.19	13.32	0.45	0.110	0.56	5	13%
37	5.96	2.295	1.995	300	338	2.92	2.67	0.25	3.19	13.32	0.45	0.105	0.56	5	11%
38	5.86	2.313	2.055	258	328	2.94	2.69	0.25	3.19	13.32	0.45	0.110	0.56	5	21%
39	5.87	2.330	2.030	300	334	2.94	2.70	0.24	3.19	13.32	0.45	0.113	0.56	5	10%
40	5.86	2.309	2.018	291	350	2.92	2.68	0.24	3.19	13.32	0.45	0.108	0.56	5	17%
41	5.92	2.458	2.168	290	353	2.92	2.69	0.23	3.19	13.32	0.45	0.110	0.56	5	18%
42	5.86	2.303	1.999	304	344	2.92	2.67	0.25	3.19	13.32	0.45	0.105	0.56	5	12%
43	5.86	2.304	2.105	199	291	2.96	2.65	0.31	3.19	13.32	0.45	0.100	0.56	5	32%
44	5.85	2.371	2.055	316	365	2.92	2.70	0.22	3.19	13.32	0.45	0.113	0.56	5	13%
45	5.93	2.495	2.185	310	420	2.92	2.75	0.17	3.19	13.32	0.45	0.125	0.56	5	26%
46	5.92	2.365	2.065	300	316	2.93	2.64	0.29	3.19	13.32	0.45	0.098	0.56	5	5%
47	5.92	2.306	2.015	291	362	2.93	2.72	0.21	3.19	13.32	0.45	0.118	0.56	5	20%
48	5.92	2.316	2.030	286	308	2.95	2.68	0.27	3.19	13.32	0.45	0.108	0.56	5	7%
49	5.95	2.324	2.065	259	299	2.96	2.69	0.27	3.19	13.32	0.45	0.110	0.56	5	13%
50	5.95	2.272	2.058	214	276	2.98	2.68	0.30	3.19	13.32	0.45	0.108	0.56	5	22%
Average	5.89	2.348	2.058	290	346	2.93	2.68	0.25	3.19	13.32	0.45	0.108	0.56	5	16%
Std	0.05	0.073	0.069	33	48	0.03	0.04	0.04	0.00	0.00	0.00	0.009	0.00	0	8%
Max	5.99	2.608	2.208	400	464	2.98	2.75	0.32	3.19	13.32	0.45	0.125	0.56	5	37%
Min	5.78	2.220	1.901	199	276	2.82	2.55	0.17	3.19	13.32	0.45	0.075	0.56	5	1%
mean	5.89	2.334	2.055	293	338	2.93	2.69	0.25	3.19	13.32	0.45	0.109	0.56	5	14%

Appendix J

The ansys simulation program flow chart